Journal of Catalysis 341 (2016) 136–148

Contents lists available at ScienceDirect

Journal of Catalysis

journal homepage: www.elsevier.com/locate/jcat

Alkanal transfer hydrogenation catalyzed by solid Brønsted acid sites

Fan Lin, Ya-Huei (Cathy) Chin *

Department of Chemical Engineering and Applied Chemistry, University of Toronto, Toronto M5S 3E5, Canada

ARTICLE INFO

Article history:
Received 10 January 2016
Revised 29 April 2016
Accepted 15 June 2016

Keywords:
Alkanal
Deoxygenation
Brønsted acid site
Zeolite
Transfer hydrogenation
Hydride transfer
Hydride ion affinity

ABSTRACT

Catalytic pathway and requirements for transfer hydrogenation of *n*-alkanals ($C_nH_{2n}O$, $n = 3–6$) on Brønsted acid sites (H^+) immobilized in microporous MFI and FAU crystalline structures or dispersed on $H_4SiW_{12}O_{40}$ polyoxometalate clusters are established by isolating its rates from those of the various concomitant catalytic cycles. Transfer hydrogenation of alkanals involves a kinetically-relevant, inter-molecular hydride transfer step from substituted tetralins or cyclohexadienes produced from the parallel alkanal coupling and ring closure reactions as the hydride donor ($R'H_2$) to protonated alkanals (RCH_2CHOH^+) as the hydride acceptor, via a bi-molecular transition state with a shared hydride ion, $(RCH_2CHOH^+\text{--}H^-\text{--}R'H^+)^\ddagger$. The rate constants for the inter-molecular hydride transfer step correlate directly to the hydride ion affinity difference between the carbenium ions of the H-donors ($R'H^+$) and the protonated alkanals (RCH_2CHOH^+). As a result, smaller alkanals with higher hydride ion affinities are more effective in abstracting hydride ions and in transfer hydrogenation ($C_4 > C_5 > C_6$). Propanal is an exception, as it is less effective in transfer hydrogenation than butanal. The deviation of propanal from the reactivity trend is apparently caused by its smaller transition state for hydride transfer, which is solvated to a lesser extent in FAU cages. The transfer hydrogenation occurs much more effectively on partially confined H^+ sites in FAU structures than in smaller pore MFI or unconfined $H_4SiW_{12}O_{40}$ polyoxometalate clusters, an indication that FAU solvates and stabilizes the bulky transition state of hydride transfer via van der Waals interactions. These effects of local site structures and the thermochemical properties of reactant determine the reactivity of alkanal transfer hydrogenation and thus selectivity ratio of alkenes, dienes, aromatics, and larger oxygenates during deoxygenation catalysis.

1. Introduction

Brønsted acid sites (H^+) immobilized on solid matrixes catalyze the deoxygenation of light alkanals (RCH_2CHO, $R = CH_3$, C_2H_5, or C_3H_7) in steps that involve inter-molecular or intra-molecular C=C bond formation, isomerization, dehydration, ring closure, and transalkylation reactions and form alkenes, dienes, alkenals, and aromatics at moderate temperatures (473–673 K) and ambient pressure, as established on H-MFI [1–4], H-Y [5], and $H_4SiW_{12}O_{40}$ polyoxometalate clusters [6]. Contained within these concurrent catalytic steps is the direct alkanal deoxygenation, which converts an alkanal reactant to the corresponding alkene ($RCH_2CHO + 2H \rightarrow RCHCH_2 + H_2O$) [1]. This reaction, in the absence of external hydrogen sources, must involve inter-molecular shuffling of hydrogen from reaction products to alkanal reactants, as required by the reaction stoichiometry. Despite the obvious involvement of reaction products as the hydrogen donors in these ubiquitous transfer hydrogenation events, their mechanism and site requirements have not been clearly established.

Brønsted acid catalyzed hydride transfer has been studied extensively with density functional theory (DFT) calculations for the transfer from alkanes to alkenes on $H_3Si{-}OH{-}AlH_2{-}O{-}SiH_3$ clusters [7–9], from alkanes (e.g., propane and *t*-butane) to alkoxides (e.g., propyl and *t*-butyl alkoxides) in mordenite zeolite [10], and from alkanes (e.g., methane and ethane) to their corresponding carbenium ions (e.g., methyl and ethyl carbenium ions) in the gas phase [11]. It has also been probed experimentally between isobutane and cyclohexene on beta and ZSM-5 zeolites and on sulfated zirconia [12], during alkane crackings in zeolites (e.g., SAPO-41, ZSM-5, and Y) [13], and during dimethyl ether homologation on $H_4SiW_{12}O_{40}$ cluster, FAU zeolite, and mesoporous SiO_2-Al_2O_3 catalysts [14]. Hydride transfer on Brønsted acid occurs when a hydride ion donor (H-donor) donates a hydride ion to the hydride ion acceptor (H-acceptor) via the formation of a carbonium ion transition state sharing the hydride ion. An example of the H-donor is an alkane and of H-acceptor is either an adsorbed carbenium ion at the H^+ site [7,8,11,15] or an alkoxide [9,10,15] at the ground state [16–18]. The transition state decomposes when the H-acceptor

---

* Corresponding author. Fax: +1 (416) 978 8605.
E-mail address: cathy.chin@utoronto.ca (Y.-H. Chin).

http://dx.doi.org/10.1016/j.jcat.2016.06.008
0021-9517/© 2016 Elsevier Inc. All rights reserved.

desorbs while the H-donor becomes a carbenium ion and then donates its proton back to the catalyst surfaces, thus regenerating the H^+ site and completing the catalytic cycle [7,8]. Local confinement of the H^+ site appears to influence the hydride transfer reactivity [13,14]: hydride transfer from n-C_5H_{12} to $C_2H_5^+$, $C_3H_7^+$, and $C_4H_9^+$ carbenium ions is most effective when occurring inside zeolites with cavity volumes of $\sim$0.2 nm^3 [e.g., CIT-1 (0.211 nm^3) and MCM-68 (0.182 nm^3)] than those with either larger [e.g., MCM-22 (0.467 nm^3) and Y (0.731 nm^3)] or smaller [e.g., SAPO-41 (0.081 nm^3) and ZSM-5 (0.131 nm^3)] cavity volumes [13]. The reaction apparently requires its bi-molecular transition state to be at comparable dimensions with those of the zeolite cavities. In fact, the sums of the volumes for ($C_2H_5^+$-n-C_5H_{10}), ($C_3H_7^+$-n-C_5H_{10}), and ($C_4H_9^+$-n-C_5H_{10}) fragments are estimated to be 0.182, 0.203, and 0.224 nm^3, respectively, in similar magnitudes with the cavities in CIT-1 and MCM-68 zeolites [13].

Large-pore FAU and BEA zeolites exhibit higher selectivities toward triptane than mesoporous SiO_2-Al_2O_3 and medium-pore MFI zeolites during solid acid catalyzed dimethyl ether homologation [14], because confinement within the larger pores preferentially solvates the larger transition states for hydride transfer and methylation and terminates the chain growth at C_7 products (triptane). Despite these extensive studies on the hydride transfer between alkanes and alkenes, few studies have addressed the hydride transfer to protonated carbonyl species. A recent study on hydrogen transfer and sequential dehydration of naphthols on H-Y zeolites has reported an increase in hydrogen transfer rates in the presence of hydrocarbons (e.g., tetralin and 1,5-dimethyltetralin), as these hydrocarbons may act as the hydrogen donors [19]. It is hypothesized that a hydride ion is being transferred from the H-donor to the keto tautomer of naphthol and the hydride ion dissociation energy of the H-donor influences the rate [19]. Little mechanistic details are available for the transfer hydrogenation of n-alkanals, despite the clear kinetic evidence of their predominant occurrences during their deoxygenation on solid Brønsted acid catalysts.

Here, we report catalytic insights and kinetic requirements for the transfer hydrogenation events, which shuffle hydrogen from H-donors, identified to be aromatic species (e.g., alkyl tetralins) or precursors to aromatics (e.g. alkyl cyclohexadienes), to protonated alkanals at Brønsted acid sites (H^+) in MFI and FAU zeolites or on polyoxometalate ($H_4SiW_{12}O_{40}$) clusters. We show that transfer hydrogenation occurs in a direct, concerted step between substituted tetralins or alkyl cyclohexadienes and protonated alkanals. The hydride donors are products of inter-molecular $C{=}C$ bond formation, ring closure, and dehydrogenation reactions. The hydride transfer reactivity exhibits a clear correlation with the hydride ion affinity differences between the carbenium ions of the H-donor and the H-acceptor and is a strong function of the extent of local structural confinements around the H^+ sites.

2. Experimental methods

2.1. Catalyst preparation

H-MFI and H-FAU zeolite samples were prepared by treating their NH_4^+ form (Zeolyst, CBV2314, 425 m^2 g^{-1}, Si/Al atomic ratio = 11.5, Na_2O = 0.05 wt.%) and H^+ form (Zeolyst, CBV720, 780 m^2 g^{-1}, Si/Al atomic ratio = 15, Na_2O = 0.03 wt.%), respectively, in flowing dry air (Linde, zero grade, 0.6 cm^3 $g_{cat.}^{-1}$ s^{-1}), by heating to 873 K at 0.0167 K s^{-1} and then holding isothermally at 873 K for 4 h. $H_4SiW_{12}O_{40}/SiO_2$ catalysts (0.075 mmol $H_4SiW_{12}O_{40}$ g_{SiO2}^{-1}) were prepared by dispersing $H_4SiW_{12}O_{40}$ (Sigma Aldrich, reagent grade, CAS #12027-43-9) on chromatographic SiO_2 (GRACE, 330 m^2 g^{-1}, 0–75 µm, 1.2 cm^3 g^{-1} pore volume, treated in air at 673 K for 5 h) via incipient wetness impregnation with a solution of $H_4SiW_{12}O_{40}$ and ethanol (Sigma-Aldrich, >99.5%, anhydrous). The impregnated $H_4SiW_{12}O_{40}/SiO_2$ samples were held in closed vials for 24 h and then treated in flowing dry air (Linde, zero grade, 0.1 cm^3 g^{-1} s^{-1}) at 323 K (0.0167 K s^{-1} heating rate) for 24 h. The H^+ site densities on these catalysts (mol H^+ $g_{cat.}^{-1}$) were measured by pyridine titration at 473 K, as described in our previous work [1].

2.2. Rate and selectivity assessments

Alkanal conversion rates and site-time-yields of alkenes, dienes, oxygenates, and aromatics were measured in a fixed bed microcatalytic quartz reactor (9.5 mm inner diameter), which was loaded with 100 mg H-MFI or H-FAU zeolites or 50 mg $H_4SiW_{12}O_{40}/SiO_2$ powders supported on a coarse quartz frit. Catalysts were treated *in-situ* under flowing He (Linde, Grade 5.0, 8.3–16.7 cm^3 $g_{cat.}^{-1}$ s^{-1}) at 0.0167 K s^{-1} to the reaction temperature (573 K) prior to rate measurements. Alkanal or butanol reactant [butanal (Sigma Aldrich, puriss grade, ⩾99%, CAS# 123-72-8), propanal (Sigma Aldrich, 97%, CAS# 123-38-6), pentanal (Sigma Aldrich, 97%, CAS# 110-62-3), hexanal (Sigma Aldrich, 98%, CAS# 66-25-1), or butanol (Sigma Aldrich, 99%, CAS# 71-36-3)] was introduced via a gas tight syringe (either 5 cm^3 Hamilton Model 1005 or 1 cm^3 SGE Model 008025), which was mounted on a syringe infusion pump (KD Scientific, LEGATO 100), into a vaporization zone heated to the boiling points of the respective reactants at atmospheric pressure, within which liquid alkanals were evaporated and mixed with He (Linde, Grade 5.0, 8.3–16.7 cm^3 $g_{cat.}^{-1}$ s^{-1}) or H_2 (Linde, Grade 5.0, 8.3 cm^3 $g_{cat.}^{-1}$ s^{-1}) purge stream. The mixture was fed to the reactor via heated transfer lines held isothermally at 473 K. Tetralin (Sigma Aldrich, 99%, CAS# 119-64-2), tetralin-adamantane mixture with a molar ratio of 20:1 (adamantane, Sigma Aldrich, 99%, CAS# 281-23-2), or cyclohexadiene (Sigma Aldrich, 97%, CAS# 592-57-4) was introduced into a second vaporization zone, which was located downstream of the zone for alkanal or alkanol vaporization described above, through a gas tight syringe (0.25 cm^3 SGE Model 006230) mounted on a syringe infusion pump (KD Scientific, LEGATO 100). This vaporization zone was maintained at 458 K for tetralin or tetralin-adamantane mixture infusion and 353 K for cyclohexadiene infusion. Chemical species in the reactor effluent stream were quantified with an online gas chromatograph (Agilent, Model 7890A) and mass spectrometer (Agilent, Model 5975C) by chromatographic separation with HP-5 (Agilent, 19091J-413, 30 m, 0.32 mm ID) or HP-5MS (Agilent, 190091S-433, 30 m, 0.25 mm ID) capillary columns. The HP-5 column was connected to thermal conductivity (TCD) and flame ionization (FID) detectors installed in series and the HP-5MS column to the mass spectrometer (MS). For each data point, the carbon balance, defined by the difference between the molar flow rates of all carbon species contained in the feed and the reactor effluent stream, was less than 10%.

3. Results and discussion

3.1. Alkanal deoxygenation pathways and the kinetic couplings of intra-molecular $C{=}C$ bond formation in alkanals and dehydrogenation of aromatic products at Brønsted acid sites

Catalytic pathways for alkanal (propanal [1,2] and butanal [6]) deoxygenation on solid Brønsted acid sites (H-MFI [1,2] and $H_4SiW_{12}O_{40}$ [6]) shown in Scheme 1 have been previously established based on selectivity changes with residence time and confirmed from reactions with the intermediates [2,6]. Butanal (C_4H_8O) deoxygenation occurs on Brønsted acid sites (H^+) via a

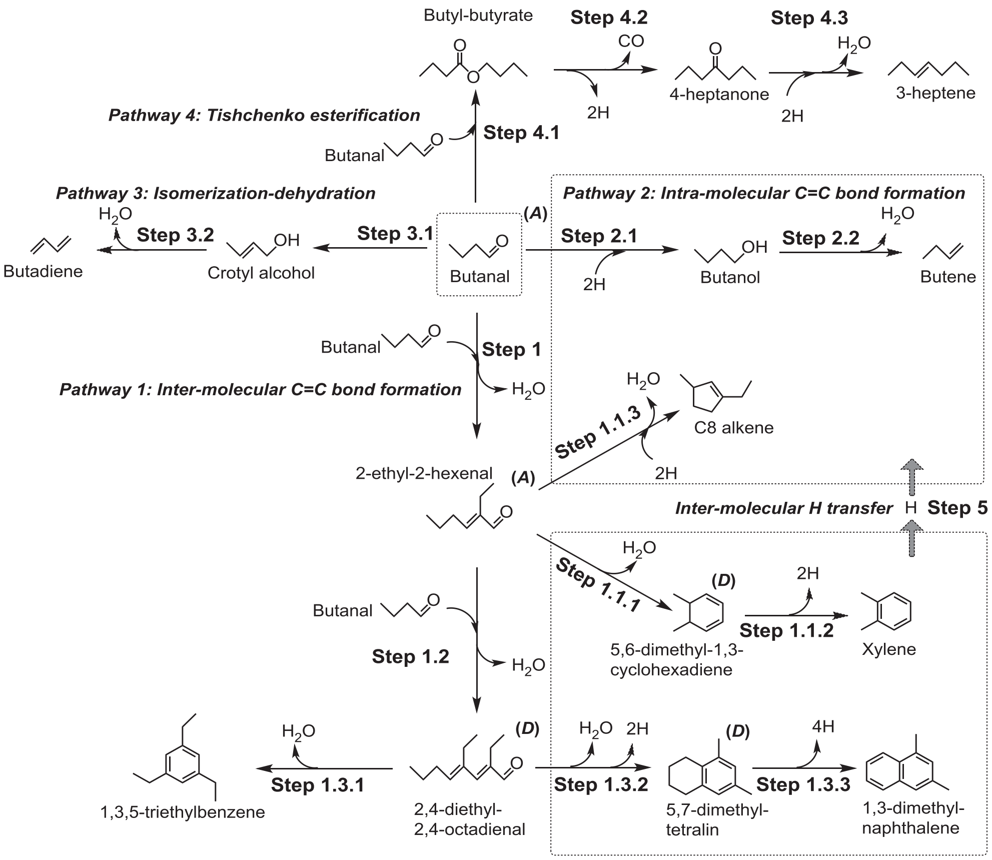

Scheme 1. Reaction network for butanal deoxygenation on solid Brønsted acid catalysts ("***D***" and "***A***" denote H-donor and H-acceptor, respectively; most of the intermediates and products shown in the scheme were detected in the experiment except crotyl alcohol and butanol because of their rapid dehydration).

bi-molecular, aldol condensation-dehydration step (Step 1, Scheme 1), which creates an inter-molecular C=C bond and forms 2-ethyl-2-hexenal ($C_8H_{14}O$), before its successive reactions with another butanal (Step 1.2) to evolve 2,4-diethyl-2,4-octadienal ($C_{12}H_{20}O$). These larger alkenals (including 2-ethyl-2-hexenal and 2,4-diethyl-2,4-octadienal) undergo sequential cyclization-dehydration (Steps 1.1.1 and 1.3.1) or cyclization-dehydration-dehydrogenation (Step 1.3.2) reaction that forms cycloalkadienes or aromatic species. Dehydrogenation of the cycloalkadienes and substituted tetralin species via Steps 1.1.2 and 1.3.3, respectively, increases their extents of unsaturation and leads to substituted benzenes (e.g., xylene) and naphthalenes (e.g., 1,3-dimethylnaphthalene), respectively, which upon transalkylation reactions evolve diverse aromatics (C_7—C_{19}, not shown in Scheme 1) [20,21]. Butanal may also undergo a primary, intra-molecular C=C bond formation, during which it accepts two H atoms followed by dehydration to evolve butene (Steps 2.1–2.2). An alternative, competitive isomerization-dehydration (Steps 3.1–3.2) of butanal leads to butadiene [22]. A small amount of basic sites in H-MFI and H-FAU zeolites (e.g., 0.05 and 0.03 wt.% Na_2O in H-MFI and H-FAU, respectively) catalyze Tishchenko esterification reaction (Step 4.1), which transforms two butanals into butyl-butyrate and sequential ketonization (Step 4.2) and hydrogenation-dehydration (Step 4.3) evolve 3-heptene [5]. The rates of Tishchenko esterification reaction (Step 4.1) increase proportionally with the number of basic sites (Fig. S1, Appendix), which include the bi-coordinated oxygen in the extra-framework alumina [23] and, for Na-exchanged H-MFI zeolites, at the conjugated oxygen of Na^+ ions [24]. Thus, this reaction occurs strictly at the basic sites. These basic sites, however, are essentially inactive for inter-molecular C=C bond formation (Step 1) at 573 K, as confirmed from the proportional decrease in its rates with the H^+ site density. As the number of H^+ sites goes to zero, the rates for inter-molecular C=C bond formation approach zero as well, despite the increase in the basic site (Na^+) density on a series of Na-exchanged H-MFI zeolites (Fig. S1a, Appendix).

These reactions occur in sequence or parallel on H-MFI, H-FAU, and $H_4SiW_{12}O_{40}/SiO_2$ catalysts. Their rates and carbon selectivities are denoted as $r_{j,m}$ and $S_{j,m}$, respectively, where subscript j represents the identity of reaction pathway (j = Inter, Intra, Dehy, or Tish, which denote inter- or intra-molecular C=C bond formation, isomerization-dehydration, or Tishchenko esterification-ketonization, respectively) and m represents the reactant (e.g., $m = C_4H_8O$). The rates of butanal conversion (r_{j,C_4H_8O}) and selectivities (S_{j,C_4H_8O}) to various pathways j on H-MFI, H-FAU, and $H_4SiW_{12}O_{40}$ were measured at 573 K and the amounts of H^+ sites remaining after the reaction at different *time-on-streams* were determined by chemical titration with pyridine (as shown in Fig. S2, Appendix). During the initial 125 min, butanal conversion rates (denoted as $r_{\text{overall},C_4H_8O}$) on H-MFI and H-FAU decreased by >72% and >47%, respectively, and the carbon selectivities (S_{j,C_4H_8O}) commensurately changed (Figs. S3a and S3b, Appendix), because of (1) the gradual occupation of the H^+ sites by butanal and (2) the loss of H^+ site (Figs. S2a and S2b, Appendix) caused by the formation of heavier products (e.g. larger aromatics and coke) inside the zeolitic pores. The rates of change for both the $r_{\text{overall},C_4H_8O}$ and S_{j,C_4H_8O} became significantly smaller above 125 min. Above 125 min, the changes in rate per unit time, defined as $\Delta r_{\text{overall},C_4H_8O}(\Delta \textit{time-on-stream})^{-1}$, were one order of magnitude smaller than the initial values and the changes in selectivity $\Delta S_{j,C_4H_8O}$ were less than ±6% over the course of 240 min for H-MFI and H-FAU (Figs. S3a and S3b, Appendix). Similarly, the number of active H^+ sites, butanal conversion rates, and carbon selectivities on $H_4SiW_{12}O_{40}$ became stable above 125 min (Figs. S2c and S3c, Appendix). Based on these time-dependent results, we conclude that butanal reactions on all three catalysts reached steady-state after 125 min. The overall butanal conversion rates, together with the rates and selectivities for each primary pathway (Pathways 1, 2, 3, and 4 in Scheme 1) at 125 min are summarized in Table 1. In the following, the rate of a primary pathway was determined from the concentration of the primary product as well as those of the secondary products resulting from the sequential reactions.

These catalysts show different selectivity values toward the different paths (Table 1). H^+ sites on $H_4SiW_{12}O_{40}$ clusters preferentially catalyze the inter-molecular C═C bond formation (Pathway 1) with a carbon selectivity of 85%, whereas H-FAU and H-MFI zeolites favor the intra-molecular C═C bond formation (Pathway 2) and isomerization-dehydration (Pathway 3) reactions, both of which involve the catalytic sojourn of a single alkanal. This is caused in a large part by the difference in the extent of H^+ site confinement (to be discussed in Section 3.3) and by the relative ratio of Brønsted acid and basic sites contained within these samples.

Both the intra-molecular C═C bond formation (Pathway 2) and isomerization-dehydration (Pathway 3) reactions involve a single butanal sojourn, during which butanal removes its oxygen heteroatom by ejecting an H_2O molecule while preserving its carbon backbone, according to the respective chemical equations of

$$C_3H_7CHO + 2H \rightarrow C_2H_5CH{=}CH_2 + H_2O \quad \text{(Pathway 2 of Scheme 1)} \tag{1}$$

$$C_3H_7CHO \rightarrow CH_2{=}CHCH{=}CH_2 + H_2O \quad \text{(Pathway 3 of Scheme 1)} \tag{2}$$

These H_2O removal steps are the predominant pathways for alkene and diene formation, confirmed from the near exclusive formation of C_nH_{2n} and C_nH_{2n-2} products from $C_nH_{2n}O$ reactants. The selectivities of C_nH_{2n} or C_nH_{2n-2} formation are expressed in terms of the molar ratios of C_nH_{2n} or C_nH_{2n-2} over the total alkene and diene fractions in the product, respectively. The selectivity values toward C_nH_{2n} were 0.95, 0.96, 0.95, and 0.92 for n equals 3, 4, 5, and 6 and toward C_nH_{2n-2} were 0.97, 0.92, and 0.91 for $n = 4$, 5 and 6, respectively (note that n of 3 is omitted here, because C_3H_6O reactions do not form C_3H_4) on H-FAU zeolites at 573 K. In addition, negligible CO and CO_2 were formed under all conditions relevant to deoxygenation reactions. The carbon selectivities toward CO and CO_2, defined by the molar ratio of carbon in CO and CO_2 over the total carbon in the products, are <4% for C_3—C_6 alkanal reactions on H-FAU (573 K), <0.03% for butanal reactions on $H_4SiW_{12}O_{40}$ (473–673 K) [6], and <3% for butanal reactions on H-MFI (573 K) over the entire operating range of our study.

The reaction stoichiometry for intra-molecular C═C bond formation (Pathway 2 of Scheme 1 and Eq. (1)) dictates that inter-molecular hydrogen transfer, which adds hydrogen atoms to the alkanals, must occur, before removal of the oxygen atom via dehydration and the eventual alkene desorption. In the absence of external hydrogen sources, hydrogen atoms are made available from the cyclization-dehydration-dehydrogenation steps (Steps 1.1.1–1.1.2, 1.3.2–1.3.3, Scheme 1). During steady state reaction, H^+ sites are occupied by alkanals (in their protonated form) as the most abundant surface intermediates. This is confirmed from the near stoichiometric butanal-to-H^+ ratios of 1.0, 1.01, and 1.1 on H-MFI (348 K), H-FAU (448 K), and $H_4SiW_{12}O_{40}$ (348 K), respectively, measured with butanal chemical titrations. Butanal adsorption and H^+ site saturation are also confirmed with Fourier transform infrared spectroscopic studies on H-FAU zeolites at 348 K; the O—H stretching bands at 3625 cm^{-1} and 3563 cm^{-1}, which correspond to the H^+ sites in the supercages and beta cages, respectively, disappear whereas the band at 1675–1685 cm^{-1} ascribed to the carbonyl stretching band of protonated butanal appears concomitantly [25]. Similarly, the infrared absorption bands of protonated carbonyl group (1670–1690 cm^{-1}) were also observed during butanal adsorption on both $H_4SiW_{12}O_{40}$ (348 K)

Table 1
Rates and selectivities for butanal deoxygenation and butanol dehydration on H-MFI, H-FAU, or $H_4SiW_{12}O_{40}$ at 573 K.

Reactant	**Reaction**	**Rate** **(Carbon selectivity)**	H-FAU[f]	H-MFI[g]	$H_4SiW_{12}O_{40}$[h]
			The rates are given in 10^{-2} mmol (mol H^+ s)$^{-1}$		
Butanal	All pathways	$r_{\text{overall},C_4H_8O}$[b]	106	35.0	1530
		(Overall conversion)	(14.3%)	(10.5%)	(18.2%)
Butanal	Pathway 1[a]: $2C_4H_8O \rightarrow C_8H_{14}O + H_2O$	r_{Inter,C_4H_8O}[b]	15.2	6.6	652
		(S_{Inter,C_4H_8O}[c])	(0.29)	(0.38)	(0.85)
Butanal	Pathway 2[a]: $C_4H_8O + 2H \rightarrow C_4H_8 + H_2O$	r_{Intra,C_4H_8O}[b]	36.0	9.6	10.0
		(S_{Intra,C_4H_8O}[c])	(0.37)	(0.27)	(0.01)
Butanal	Pathway 3[a]: $C_4H_8O \rightarrow C_4H_6 + H_2O$	r_{Dehy,C_4H_8O}[b]	1.0	4.5	29.2
		(S_{Dehy,C_4H_8O}[c])	(0.01)	(0.13)	(0.02)
Butanal	Pathway 4[a]: $2C_4H_8O \rightarrow C_7H_{14} + CO + H_2O$	r_{Tish,C_4H_8O}[b, d] in 10^{-5} mmol ($g_{\text{cat.}}$ s)$^{-1}$	7.4	0.9	1.2
		(S_{Tish,C_4H_8O}[c])	(0.27)	(0.05)	(0.01)
1-Butanol	$C_4H_9OH \rightarrow C_4H_8 + H_2O$	r_{Dehy,C_4H_9OH}[e]	–	>370	>4400
		Rate ratio			
		$r_{\text{Dehy},C_4H_9OH}(r_{\text{Intra},C_4H_8O})^{-1}$	–	>38	>440

[a] Pathways 1, 2, 3, and 4 denote the reaction pathways (in Scheme 1) of inter-molecular C═C bond formation (Step 1), intra-molecular C═C bond formation (Steps 2.1–2.2), isomerization-dehydration (Steps 3.1–3.2), and Tishchenko esterification-ketonization (Steps 4.1–4.3), respectively.

[b] $r_{\text{overall},C_4H_8O}$ denotes the overall C_4H_8O conversion rate; r_{j,C_4H_8O} represents the rate of reaction for pathway j during C_4H_8O deoxygenation (subscript j = Inter, Intra, Dehy, or Tish, which denote inter- or intra-molecular C═C bond formation, isomerization-dehydration, or Tishchenko esterification-ketonization, respectively).

[c] S_{j,C_4H_8O} represents the selectivity to pathway j during C_4H_8O deoxygenation, defined as the rate of C_4H_8O consumption in reaction j divided by the overall C_4H_8O conversion rate (subscript j = Inter, Intra, Dehy, Tish, which denote inter- or intra-molecular C═C bond formation, isomerization-dehydration, or Tishchenko esterification-ketonization, respectively).

[d] Because Pathway 4 occurs on the basic sites, the unit for r_{Tish,C_4H_8O} is given in terms of 10^{-5} mmol ($g_{\text{cat.}}$ s)$^{-1}$, cat. = H-MFI, H-FAU, or $H_4SiW_{12}O_{40}$.

[e] The rate of 1-butanol (C_4H_9OH) dehydration, r_{Dehy,C_4H_9OH}, was measured with 1.1 kPa 1-butanol, space velocity 0.0033 and 0.045 mol 1-butanol (mol H^+ s)$^{-1}$ on H-MFI and $H_4SiW_{12}O_{40}$, respectively.

[f] Si/Al = 11.5, space velocity 0.0033 mol butanal (mol H^+ s)$^{-1}$, 1.1 kPa butanal, *time-on-stream* = 125 min.

[g] Si/Al = 15, space velocity 0.0074 mol butanal (mol H^+ s)$^{-1}$, 1.1 kPa butanal, *time-on-stream* = 125 min.

[h] 0.075 mmol $H_4SiW_{12}O_{40}$ $g_{SiO_2}^{-1}$, space velocity 0.045 mol butanal (mol H^+ s)$^{-1}$, 1.1 kPa butanal, *time-on-stream* = 125 min.

clusters and H-MFI zeolites (313 K), accompanied by the disappearance of the O—H bands [25]. On such surfaces, the rates of intra-molecular C=C bond formation (r_{Intra,C_4H_8O}, per H$^+$ site), which also equal the site-time-yields of butene, increase linearly with the total pressure of the aromatic fraction ($P_{\text{Aromatics}}$), as shown in Fig. 1 for butanal deoxygenation on H-MFI, H-FAU, and $H_4SiW_{12}O_{40}$ at 573 K. Butanal conversions and partial pressures did not influence the rates for intra-molecular C=C bond formation and their dependences, because these changes on H$^+$ sites that are saturated with either butanals or their isomers alter neither the identity nor the coverages of the most abundant surface intermediates during steady-state reactions. This dependence suggests the catalytic involvement of aromatic species as H-donors. The aromatic fraction contains alkyl benzenes and alkyl tetralins (e.g., $C_{12}H_{18}$ and $C_{12}H_{16}$, respectively), produced from the cyclization-dehydration (Step 1.3.1) or cyclization-dehydration-dehydrogenation (Step 1.3.2) of alkenal species. These alkyl benzenes and alkyl tetralins donate their hydrogen atoms and thus further increase their extents of saturation, forming either alkenyl benzenes or alkyl naphthalenes. Figs. 2a and 2b shows the carbon distributions among the aromatic products on H-FAU at different space velocities, whereas Figs. 2c and 2d depicts the carbon distributions on H-MFI and $H_4SiW_{12}O_{40}$, respectively. The different distributions are results from the different extents in secondary dehydrogenation and transalkylation reactions. For example, dehydrogenation of C_8 alkyl cyclohexadienes (C_8H_{12}), C_{13} alkyl benzenes ($C_{13}H_{20}$), and C_{16} alkyl tetralins ($C_{16}H_{24}$) forms xylenes (C_8H_{10}), alkyl naphthalenes ($C_{13}H_{14}$), and C_{16} alkyl naphthalenes ($C_{16}H_{20}$), respectively. As the space velocity decreases from 0.030 mol butanal (mol H$^+$ s)$^{-1}$ to 0.0074 mol butanal (mol H$^+$ s)$^{-1}$, the fractions of C_8H_{10}, $C_{13}H_{14}$, and $C_{16}H_{20}$ in the aromatic products increase from 2.6%, 8.5%, and 8.3% to 6.3%, 10.5%, and 11.8%, (Figs. 2a and 2b) because the lower space velocity and longer contact time favor the secondary dehydrogenation reactions. The carbon distributions also vary among the different catalysts (Figs. 2b–2d), because of the different extents of H$^+$ site confinement, to be discussed in Section 3.3.

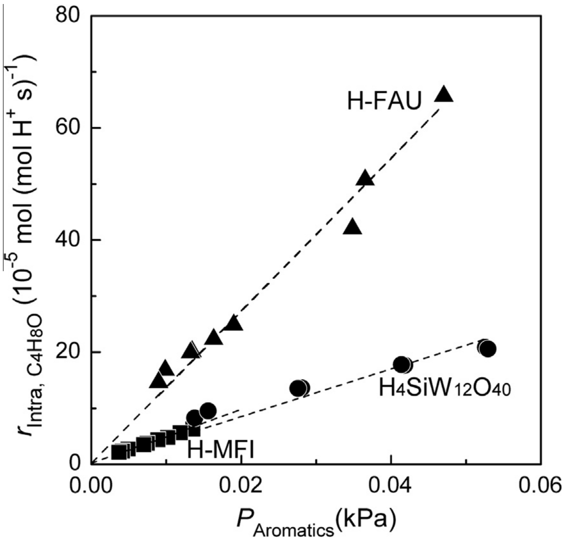

Fig. 1. Rates for intra-molecular C=C bond formation (Pathway 2, r_{Intra,C_4H_8O}) as a function of aromatic pressure ($P_{\text{Aromatics}}$) during butanal reactions on H-MFI [■, Si/Al = 11.5, space velocity 0.0033–0.013 mol butanal (mol H$^+$ s)$^{-1}$], H-FAU [▲, Si/Al = 15, space velocity 0.0074–0.03 mol butanal (mol H$^+$ s)$^{-1}$], and $H_4SiW_{12}O_{40}$ [●, 0.075 mmol $H_4SiW_{12}O_{40}$ $g_{SiO_2}^{-1}$, space velocity 0.045–0.18 mol butanal (mol H$^+$ s)$^{-1}$] at 573 K.

The rate dependencies for intra-molecular C=C bond formation (r_{Intra,C_4H_8O}) on H$^+$ sites predominantly occupied by protonated butanals (Fig. 1) are consistent with kinetically-relevant transfer hydrogenation, which shuffles a hydrogen atom from the H-donor (denoted as D) to a protonated butanal (see derivation and full rate equation in Eqs. (S1.1)–(S1.7), Sec. S1 of Appendix). The rate equation, upon simplification, shows that the rate for butanal transfer hydrogenation, r_{TH,C_4H_8O-D}, increases linearly with the hydrogen donor pressure, P_D:

$$r_{\text{TH},C_4H_8O-D} = k_{\text{TH},C_4H_8O-D}P_D \tag{3}$$

where k_{TH,C_4H_8O-D} is the rate constant for transfer hydrogenation. The linear relations in Fig. 1 suggest that either aromatics (e.g., methyl- or ethyl-substituted tetralins) or precursors to aromatics (e.g., 5,6-dimethyl-1,3-cyclohexadiene) act as the H-donors. The transfer hydrogenation involves cooperative dehydrogenation (Steps 1.1.2 and 1.3.2–1.3.3) of the H-donors (labeled "***D***" in Scheme 1) and intra-molecular C=C bond formation (Steps 2.1–2.2) of butanal, the H-acceptor (labeled "***A***" in Scheme 1). The reaction leads to alkyl naphthalenes (or alkyl benzenes) and butene. Only a portion of the aromatic products or precursors of aromatics can act as H-donors, and depending on their chemical identity, the transfer hydrogenation rate constant k_{TH,C_4H_8O-D} varies accordingly. Assuming β_y is the fraction of a specific H-donor D_y within the aromatic products (where subscript y denotes the chemical identity) and $k_{\text{TH},C_4H_8O-D_y}$ is the rate constant for transfer hydrogenation between D_y and butanal, the rate for intra-molecular C=C bond formation, r_{Intra,C_4H_8O}, is:

$$r_{\text{Intra},C_4H_8O} = \sum_{y=1}^{t} k_{\text{TH},C_4H_8O-D_y}\beta_y P_{\text{Aromatics}} = k_{\text{Intra},C_4H_8O}P_{\text{Aromatics}} \tag{4a}$$

$$k_{\text{Intra},C_4H_8O} = \sum_{y=1}^{t} k_{\text{TH},C_4H_8O-D_y}\beta_y \tag{4b}$$

According to Eq. (4a), r_{Intra,C_4H_8O} increases linearly with the total aromatic pressure ($P_{\text{Aromatics}}$), consistent with the rate dependency shown in Fig. 1. k_{Intra,C_4H_8O} is the effective rate constant for intra-molecular C=C bond formation, and it depends on the fraction of H-donors within the aromatics (β_y) and the transfer hydrogenation rate constants ($k_{\text{TH},C_4H_8O-D_y}$) of the various H-donors (D_y, y = 1, 2, ...), as shown in Eq. (4b).

The slopes in Fig. 1 reflect the rate constants k_{Intra,C_4H_8O} on different catalysts. The rate constant values were higher on H-FAU than on H-MFI and $H_4SiW_{12}O_{40}$ [k_{Intra,C_4H_8O} = 13.6 ± 0.3 mmol (mol H$^+$ s kPa)$^{-1}$ on H-FAU vs. 5.8 ± 0.3 and 4.3 ± 0.2 mmol (mol H$^+$ s kPa)$^{-1}$ on H-MFI and $H_4SiW_{12}O_{40}$, respectively, 573 K], indicating that transfer hydrogenation events occur much more effectively on partially confined, large pore H-FAU zeolites and less so on medium pore H-MFI zeolites and unconfined structure of $H_4SiW_{12}O_{40}$ clusters. The different reactivities in transfer hydrogenation among the H-FAU, H-MFI, and $H_4SiW_{12}O_{40}$ catalysts could be caused either by the difference in H$^+$ site environments among the catalysts or in H-donor identities. In order to decouple these different contributions, we incorporated either tetralin or cyclohexadiene as the H-donor into the alkanal reactions and then isolated the rates for tetralin-to-alkanal or cyclohexadiene-to-alkanal transfer hydrogenation by subtracting the rate contributions of aromatic products from the total transfer hydrogenation rates, as discussed next in Sections 3.2 and 3.3.

3.2. Mechanism of transfer hydrogenation between tetralins or cyclohexadienes and protonated alkanals at Brønsted acid sites

The transfer hydrogenation between substituted tetralins or cyclohexadienes and protonated butanals was probed and confirmed by incorporating tetralin, tetralin-adamantane mixture, or cyclohexadiene in the butanal feed during steady-state butanal

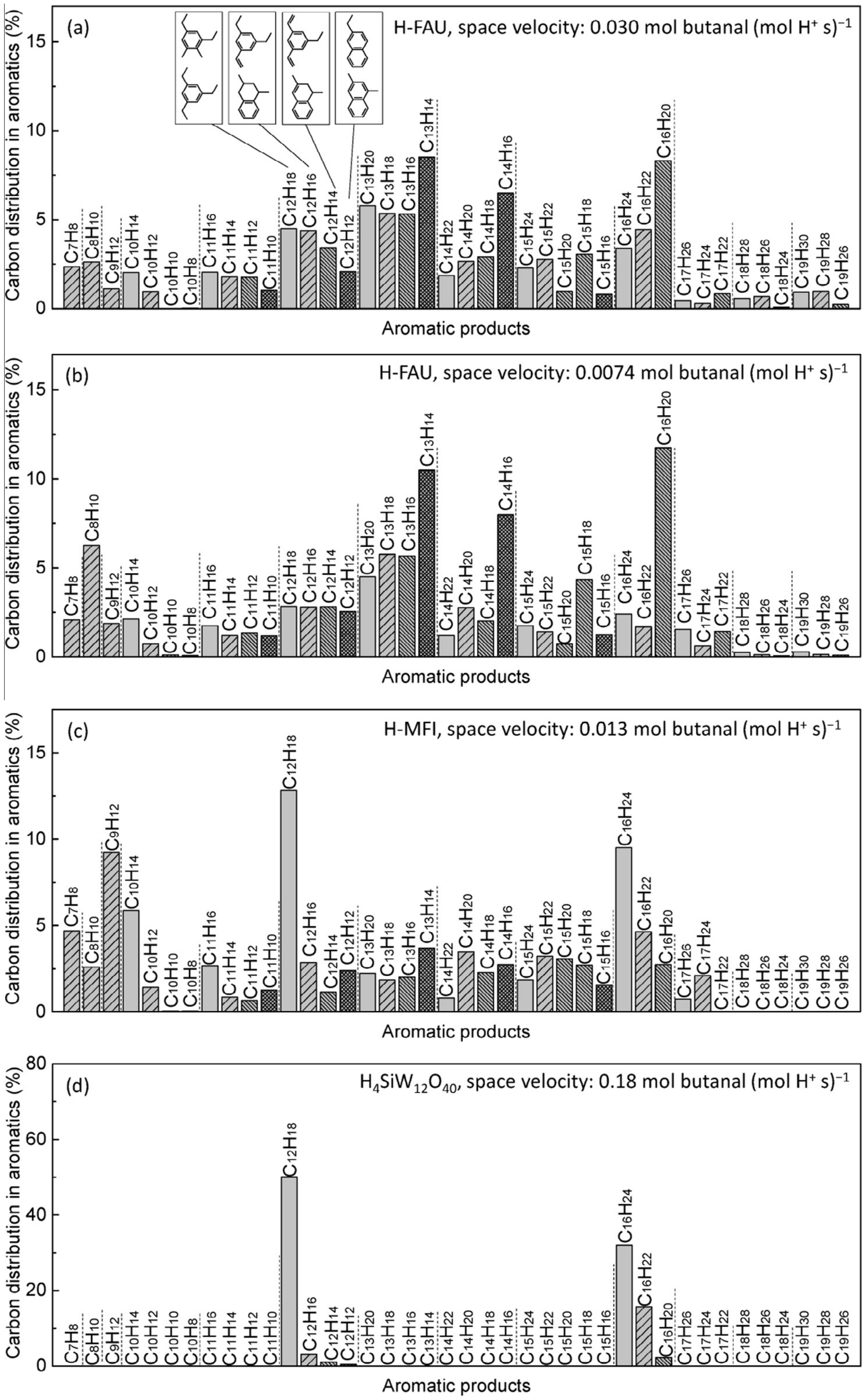

Fig. 2. Carbon distributions of aromatic fraction produced in butanal reactions on (a and b) H-FAU with different space velocities, (c) H-MFI, and (d) $H_4SiW_{12}O_{40}$ at 573 K at *time-on-stream* of 125 min. The distributions include aromatic molecules that do not lose any H (▢) or lose 2 (▨), 4 (▧), or 6 (▩) hydrogen atoms in dehydrogenation reactions (e.g., Steps 1.1.2 and 1.3.3, Scheme 1).

deoxygenation reactions. Tetralin ($C_{10}H_{12}$) and cyclohexadiene (C_6H_8, denoted as chd) are known as effective hydrogen donors, because of their strong thermodynamic tendencies toward dehydrogenation, leading to naphthalene and benzene, respectively, with more effective π-electron delocalization [26], whereas adamantane (denoted as ad) is used as a co-catalyst in the transfer hydrogenation reaction [27]. The rate of each reaction *j* (*j* = Inter, Intra, Dehy, or Tish) was measured on H-FAU, H-MFI, and $H_4SiW_{12}O_{40}$ at 573 K while incorporating tetralin (0.08–0.16 kPa), tetralin-adamantane (0.08–0.16 kPa tetralin and 4–8 Pa adaman-

Table 2
The extent of promotion, $\alpha_{j,\mathrm{tetralin}}$, $\alpha_{j,\mathrm{tetralin\text{-}ad}}$, or $\alpha_{j,\mathrm{chd}}$ for the various reactions j (j = Inter, Intra, Dehy, or Tish) with tetralin, tetralin-adamantane, or cyclohexadiene incorporation during butanal deoxygenation, and the rate constant for cyclohexadiene-to-butanal transfer hydrogenation, $k_{\mathrm{TH,C_4H_8O-chd}}$, on H-FAU, H-MFI, and $H_4SiW_{12}O_{40}$ at 573 K.

Reaction		H-FAU	H-MFI	$H_4SiW_{12}O_{40}$
	Extent of promotion		kPa^{-1}	
Pathway 1[a]: $2C_4H_8O \rightarrow C_8H_{14}O + H_2O$	$\alpha_{\mathrm{Inter,tetralin}}$[b]	−0.4 ± 0.2	1.4 ± 0.1	0.4 ± 0.2
	$\alpha_{\mathrm{Inter,tetralin\text{-}ad}}$[b]	−0.5 ± 0.3	–	–
	$\alpha_{\mathrm{Inter,chd}}$[b]	1.2 ± 0.6	1.2 ± 0.7	−0.9 ± 0.3
Pathway 2[a]: $C_4H_8O + 2H \rightarrow C_4H_8 + H_2O$	$\alpha_{\mathrm{Intra,tetralin}}$[b]	16.1 ± 0.2	1.3 ± 0.2	0.7 ± 0.3
	$\alpha_{\mathrm{Intra,tetralin\text{-}ad}}$[b]	23.7 ± 0.6	–	–
	$\alpha_{\mathrm{Intra,chd}}$[b]	29.0 ± 2.0	14.4 ± 0.8	9.2 ± 0.3
Pathway 3[a]: $C_4H_8O \rightarrow C_4H_6 + H_2O$	$\alpha_{\mathrm{Dehy,tetralin}}$[b]	−8.3 ± 0.1	0.1 ± 0.1	0 ± 0.3
	$\alpha_{\mathrm{Dehy,tetralin\text{-}ad}}$[b]	−6.9 ± 0.1	–	–
	$\alpha_{\mathrm{Dehy,chd}}$[b]	−6.9 ± 0.4	−28.6 ± 1.0	0.6 ± 0.3
Pathway 4[a]: $2C_4H_8O \rightarrow C_7H_{14} + CO + H_2O$	$\alpha_{\mathrm{Tish,tetralin}}$[b]	−1.3 ± 0.3	−0.4 ± 0.3	1.9 ± 0.4
	$\alpha_{\mathrm{Tish,tetralin\text{-}ad}}$[b]	−0.6 ± 0.1	–	–
	$\alpha_{\mathrm{Tish,chd}}$[b]	0 ± 0.3	−1.1 ± 0.7	−0.8 ± 0.8
	Rate constant		mmol (mol H^+ s kPa)$^{-1}$	
$C_4H_8O + C_6H_8 \rightarrow C_4H_8 + C_6H_6 + H_2O$	$k_{\mathrm{TH,C_4H_8O-chd}}$[c]	6.8 ± 0.3	2.8 ± 0.4	0.52 ± 0.03

[a] Pathways 1, 2, 3, and 4 denote the reaction pathways (in Scheme 1) of inter-molecular C=C bond formation (Step 1), intra-molecular C=C bond formation (Steps 2.1–2.2), isomerization-dehydration (Steps 3.1–3.2), and Tishchenko esterification-ketonization (Steps 4.1–4.3), respectively.

[b] The $\alpha_{j,m}$ values (j = Inter, Intra, Dehy, or Tish; m = tetralin, tetralin-ad, or chd) are the slopes obtained by linear regression of the data points in Figs. 3a, 3b, or 3c against Eqs. (5a), (5b), or (5c), respectively.

[c] The rate constants for cyclohexadiene-to-butanal transfer hydrogenation, $k_{\mathrm{TH,C_4H_8O-chd}}$, were measured on H-FAU, H-MFI, and $H_4SiW_{12}O_{40}$ at 573 K, with space velocities of 0.0074, 0.0033, and 0.045 mol butanal (mol H^+ s)$^{-1}$, respectively.

tane), or cyclohexadiene (0.03–0.15 kPa) into the butanal feed. These rates with tetralin, tetralin-adamantane, or cyclohexadiene incorporation ($r_{j,\mathrm{C_4H_8O-tetralin}}$, $r_{j,\mathrm{C_4H_8O-tetralin\text{-}ad}}$, or $r_{j,\mathrm{C_4H_8O-chd}}$, respectively), when divided by those in pure butanal feed ($r_{j,\mathrm{C_4H_8O}}$), give the rate ratios $r_{j,\mathrm{C_4H_8O-tetralin}}(r_{j,\mathrm{C_4H_8O}})^{-1}$, $r_{j,\mathrm{C_4H_8O-tetralin\text{-}ad}}(r_{j,\mathrm{C_4H_8O}})^{-1}$, or $r_{j,\mathrm{C_4H_8O-chd}}(r_{j,\mathrm{C_4H_8O}})^{-1}$, respectively. These rate ratios are linear functions of either tetralin pressure (P_{tetralin}) or cyclohexadiene pressure (P_{chd}), as shown in Fig. 3 for H-FAU zeolites according to

$$\frac{r_{j,\mathrm{C_4H_8O-tetralin}}}{r_{j,\mathrm{C_4H_8O}}} = 1 + \alpha_{j,\mathrm{tetralin}} P_{\mathrm{tetralin}} \tag{5a}$$

$$\frac{r_{j,\mathrm{C_4H_8O-tetralin\text{-}ad}}}{r_{j,\mathrm{C_4H_8O}}} = 1 + \alpha_{j,\mathrm{tetralin\text{-}ad}} P_{\mathrm{tetralin}} \tag{5b}$$

$$\frac{r_{j,\mathrm{C_4H_8O-chd}}}{r_{j,\mathrm{C_4H_8O}}} = 1 + \alpha_{j,\mathrm{chd}} P_{\mathrm{chd}} \tag{5c}$$

where $\alpha_{j,\mathrm{tetralin}}$, $\alpha_{j,\mathrm{tetralin\text{-}ad}}$, and $\alpha_{j,\mathrm{chd}}$ are the proportionality constants and also the slopes of the data points in Fig. 3. Their values reflect the extents of promotion for the various reactions j (j = Inter, Intra, Dehy, or Tish) with tetralin, tetralin-adamantane, or cyclohexadiene incorporation, as summarized in Table 2. For example, the positive $\alpha_{\mathrm{Intra,tetralin}}$ and negative $\alpha_{\mathrm{Dehy,tetralin}}$ values of 16.1 ± 0.2 and −8.3 ± 0.1 kPa^{-1}, respectively, on H-FAU zeolites indicate that tetralin promotes the rate for Pathway 2 ($r_{\mathrm{Intra,C_4H_8O}}$) and inhibits the rate for Pathway 3 ($r_{\mathrm{Dehy,C_4H_8O}}$). In contrast, smaller values of $\alpha_{\mathrm{Inter,tetralin}}$ (−0.4 ± 0.2 kPa^{-1}) and $\alpha_{\mathrm{Tish,tetralin}}$ (−1.3 ± 0.3 kPa^{-1}) on H-FAU correspond to rate changes of less than 10%; these smaller alpha values indicate that Pathway 1 ($r_{\mathrm{Inter,C_4H_8O}}$) and Pathway 4 ($r_{\mathrm{Tish,C_4H_8O}}$) are barely influenced by tetralin.

The rate ratio $r_{\mathrm{Intra,C_4H_8O-tetralin}}(r_{\mathrm{Intra,C_4H_8O}})^{-1}$ for intra-molecular C=C bond formation on H-FAU zeolites increased with tetralin pressure, thus $\alpha_{\mathrm{Intra,tetralin}}$ acquired a positive value of 16.1 ± 0.2 kPa^{-1}. Incorporation of 4–8 Pa adamantane at an adamantane-to-tetralin ratio of 1:20 increased the transfer hydrogenation events and the corresponding $\alpha_{\mathrm{Intra,tetralin\text{-}ad}}$ value further to 23.7 ± 0.6 kPa^{-1}, because adamantane acts as a H transfer co-catalyst that donates its tertiary H-atom to form an adamantyl

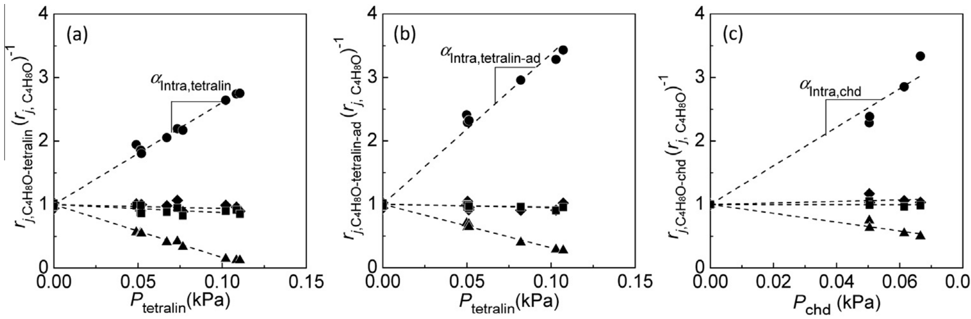

Fig. 3. Rate ratios [$r_{j,\mathrm{C_4H_8O-tetralin}}(r_{j,\mathrm{C_4H_8O}})^{-1}$, $r_{j,\mathrm{C_4H_8O-tetralin\text{-}ad}}(r_{j,\mathrm{C_4H_8O}})^{-1}$, or $r_{j,\mathrm{C_4H_8O-chd}}(r_{j,\mathrm{C_4H_8O}})^{-1}$] for the rates of butanal primary reactions in (a) C_4H_8O-tetralin ($r_{j,\mathrm{C_4H_8O-tetralin}}$), (b) C_4H_8O-tetralin-adamantane ($r_{j,\mathrm{C_4H_8O-tetralin\text{-}ad}}$), or (c) C_4H_8O-cyclohexadiene ($r_{j,\mathrm{C_4H_8O-chd}}$) feed mixtures to those in C_4H_8O feed ($r_{j,\mathrm{C_4H_8O}}$) as a function of tetralin pressure (P_{tetralin}) or cyclohexadiene pressure (P_{chd}) for inter-molecular C=C bond formation (Pathway 1, ◆), intra-molecular C=C bond formation (Pathway 2, ●), isomerization-dehydration (Pathway 3, ▲), and Tishchenko esterification-ketonization (Pathway 4, ■) on H-FAU at 573 K [subscript j = Inter, Intra, Dehy, or Tish, which denote inter- or intra-molecular C=C bond formation, isomerization-dehydration, or Tishchenko esterification-ketonization, respectively; space velocity 0.0074 mol butanal (mol H^+ s)$^{-1}$, adamantane (if added) = 4–8 Pa]. The $\alpha_{j,m}$ values (j = Inter, Intra, Dehy, or Tish; m = tetralin, tetralin-ad, or chd) are determined from the slopes in these figures by linear regression of the data points against either Eqs. (5a), (5b), or (5c), and are summarized in Table 2.

Table 3
Rates for tetralin dehydrogenation and butanal hydrogenation on H-FAU and $H_4SiW_{12}O_{40}$ at 573 K.

Reactants	Butanal (1.1 kPa)-tetralin (0.08 kPa)		Tetralin (0.08 kPa)	Butanal (1.1 kPa)-H_2 (99 kPa)
Reactions	Step A: $C_{10}H_{12} + 2C_4H_8O \rightarrow C_{10}H_8 + 2C_4H_8 + 2H_2O$ Step B1: $C_{10}H_{12} \rightarrow C_{10}H_8 + 2H_2$		Step B1: $C_{10}H_{12} \rightarrow C_{10}H_8 + 2H_2$	Step B2: $C_4H_8O + H_2 \rightarrow C_4H_8 + H_2O$
Rate	$r_{DH,C_4H_8O-tetralin}$[a] (Steps A and B1)	$r_{TH,C_4H_8O-tetralin}$[b] (Step A)	$r_{DH,tetralin}$[a] (Step B1)	$r_{Hydro,C_4H_8O-H_2}$[c] (Step B2)
H-FAU	0.35 ± 0.03	0.27 ± 0.02	0.13 ± 0.01	~0.007
$H_4SiW_{12}O_{40}$	0.022 ± 0.002	<detection limit[d]	Unavailable	<detection limit[d]

[a] Rate of tetralin ($C_{10}H_{12}$) dehydrogenation, $r_{DH,m}$ (subscript m denotes either C_4H_8O-tetralin feed mixture or tetralin), is defined as the rate of naphthalene ($C_{10}H_8$) formation via Step A and/or Step B1, and given in mmol $C_{10}H_8$ (mol H^+ s)$^{-1}$; space velocity 5.4×10^{-4} and 3.3×10^{-3} mol tetralin (mol H^+ s)$^{-1}$ for H-FAU and $H_4SiW_{12}O_{40}$, respectively.

[b] Rate of C_4H_8O transfer hydrogenation, $r_{TH,C_4H_8O-tetralin}$, is the rate of C_4H_8O hydrogenation via Step A in C_4H_8O-tetralin feed mixture, and is determined according to Eq. (8), given in mmol C_4H_8 (mol H^+ s)$^{-1}$; space velocity 0.0074 and 0.045 mol butanal (mol H^+ s)$^{-1}$ for H-FAU and $H_4SiW_{12}O_{40}$, respectively.

[c] Rate of C_4H_8O transfer hydrogenation by H_2, $r_{Hydro,C_4H_8O-H_2}$, in C_4H_8O-H_2 feed mixture, is given in mmol C_4H_8 (mol H^+ s)$^{-1}$; space velocity 0.0074 and 0.045 mol butanal (mol H^+ s)$^{-1}$ for H-FAU and $H_4SiW_{12}O_{40}$, respectively.

[d] Below the detection limit.

cation [27,28], which subsequently abstracts a hydride ion from the tetralin to complete its catalytic cycle. These additional transfer hydrogenation events as a result of tetralin addition were confirmed from comparable rates for naphthalene ($C_{10}H_8$) formation (from tetralin dehydrogenation) and for incremental butene formation. The naphthalene formation rate is 0.35 ± 0.03 mmol $C_{10}H_8$ (mol H^+ s)$^{-1}$ with 0.08 kPa tetralin and 1.1 kPa butanal at 573 K on H-FAU, which corresponds to a H donation rate of 1.4 ± 0.12 mmol H (mol H^+ s)$^{-1}$, as each $C_{10}H_8$ turnover donates 4 H atoms (Table 3, Steps A and B1). The incremental rate of butene formation resulted from the tetralin addition, which equals the rate of butanal transfer hydrogenation by tetralin ($r_{TH,C_4H_8O-tetralin}$), was determined by subtracting the rate of butene formation with C_4H_8O feed from that with C_4H_8O-tetralin mixture ($r_{TH,C_4H_8O-tetralin} = \Delta r_{Intra} = r_{Intra,C_4H_8O-tetralin} - r_{Intra,C_4H_8O}$). The transfer hydrogenation rate, $r_{TH,C_4H_8O-tetralin}$, was found to be 0.27 ± 0.02 mmol C_4H_8 (mol H^+ s)$^{-1}$ on H-FAU (Table 3, Step A), which translates to a H acceptance rate of 0.54 ± 0.04 mmol H (mol H^+ s)$^{-1}$, as each C_4H_8 formation requires 2 H atoms. This increment in butene formation rates ($r_{Intra,C_4H_8O-tetralin} > r_{Intra,C_4H_8O}$) and the concomitant detection of naphthalene upon tetralin addition confirm the involvement of tetralin as the hydrogen donor. Transfer hydrogenation from alkanes to alkenes has been previously proposed to involve a hydride ion transfer step at Brønsted acid sites, as established on acidic zeolites based on density functional theory calculations carried out on a cluster model, H_3-Si—OH—AlH_2—O—SiH_3 [7–9]. The hydride transfer reaction involves an initial alkene protonation that forms a carbenium ion at the H^+ site ($C_nH_{2n} + H^+ \rightarrow C_nH_{2n+1}^+$). The carbenium ion then accepts a hydride ion from an alkane (C_mH_{2m+2}) via the formation of a carbonium ion ($C_nH_{2n+1}^+$--H^---$C_mH_{2m+1}^+$)‡ transition state, followed by its decomposition into an alkane (C_nH_{2n+2}) and a carbenium ion ($C_mH_{2m+1}^+$). The carbenium ion ($C_mH_{2m+1}^+$) then donates a proton to the zeolitic framework in order to restore the Brønsted acid site (H^+) and desorbs as alkene, C_mH_{2m}. We propose a similar mechanism for the transfer hydrogenation involving tetralin ($C_{10}H_{12}$) and butanal (C_4H_8O) as a hydride donor and acceptor pair at the Brønsted acid site, as shown in Scheme 2. Initially, a butanal adsorbs on a H^+ site as protonated $C_4H_8OH^+$ (Step I) and, as a result, its carbonyl functional group becomes polarized and the carbonyl carbon acts as a hydride acceptor [29]. The protonated butanal $C_4H_8OH^+$ then accepts a hydride ion from tetralin ($C_{10}H_{12}$) in a concerted step via a carbonium ion transition state ($C_4H_8OH^+$--H^---$C_{10}H_{11}^+$)‡ (Step II), which upon decomposition, leads to a butanol (C_4H_9OH) molecule and tetralin carbenium ion ($C_{10}H_{11}^+$) (Step III). The carbenium ion of tetralin ($C_{10}H_{11}^+$) donates a H^+ to the zeolitic framework and forms 1,2-dihydronaphthalene ($C_{10}H_{10}$), thus regenerating the Brønsted acid site (Step IV) and completing the catalytic cycle. Butanol then undergoes sequential rapid, kinetically-irrelevant acid catalyzed dehydration reaction (Step V) that evolves butene (C_4H_8). The kinetic irrelevance of the butanol dehydration step (Step 2.2 in Scheme 1 and Step V in Scheme 2) is confirmed from the much higher rates for butanol dehydration (r_{Dehy,C_4H_9OH}) than for intra-molecular C=C bond formation (r_{Intra,C_4H_8O}): the rate ratio for butanol dehydration to the intra-molecular C=C bond formation in butanal, $r_{Dehy,C_4H_9OH}\left(r_{Intra,C_4H_8O}\right)^{-1}$, measured at either 1.1 kPa butanol or butanal, exceeds 38 on H-MFI and 440 on $H_4SiW_{12}O_{40}$ at 573 K, as summarized in Table 1.

Butadiene (C_4H_6) instead of butene may form as a side product from the direct dehydration of butanal (Pathway 3). The direct dehydration reaction was proposed to occur via allylic alcohol intermediates [30], as confirmed from the similar yields for the conversions of 2-methylbutanal and its isomer, methyl isopropyl ketone, to a common intermediate, 2-methyl-2-buten-1-ol, before its dehydration to isoprene on $AlPO_4$. The yields toward isoprene from 2-methylbutanal and methyl isopropyl ketone are 49% and 54%, respectively, which are very similar. The primary isomerization-dehydration reaction (Steps 3.1–3.2 in Scheme 1 and Eq. (2)) converts butanal to crotyl alcohol before its sequential dehydration to butadiene, according to

$$C_3H_7CHO \rightarrow CH_3{-}CH{=}CH{-}CH_2OH \quad \text{(also in Step 3.1 of Scheme 1)} \tag{6a}$$

$$CH_3{-}CH{=}CH{-}CH_2OH \rightarrow CH_2{=}CHCH{=}CH_2 + H_2O \quad \text{(also in Step 3.2 of Scheme 1)} \tag{6b}$$

Incorporation of tetralin decreased the net rate of butadiene formation ($r_{Dehy,C_4H_8O-tetralin} < r_{Dehy,C_4H_8O}$), as shown in Figs. 3a and 3b, and led to negative $\alpha_{Dehy,tetralin}$ and $\alpha_{Dehy,tetralin\text{-}ad}$ values (Eqs. (5a) and (5b)) of −8.3 ± 0.1 kPa^{-1} and −6.9 ± 0.1 kPa^{-1}, respectively. Such decreases are caused either by tetralin inhibiting the isomerization-dehydration reaction or by the sequential reaction of butadiene with tetralin. We rule out the former reason because tetralin did not perturb the concurrent primary pathways (Pathways 1 and 4, Scheme 1), an indication that its addition did not alter the identity of the most abundant surface intermediate. We hypothesize that butadiene undergoes transfer hydrogenation, during which it accepts two hydrogen atoms from tetralin and converts to butene ($C_4H_6 + C_{10}H_{12} \rightarrow C_4H_8 + C_{10}H_{10}$), thus decreasing the net rate of butadiene formation. In fact, the hydride ion affinity (*HIA*) for protonated butadiene ($C_4H_7^+$) is higher than the carbenium ion of tetralin ($C_{10}H_{11}^+$) (*HIA* = 1011.5 kJ mol^{-1} for $C_4H_7^+$ vs. 934.1 kJ mol^{-1} for $C_{10}H_{11}^+$, Table S1, in Sec. S3 of Appendix), making the transfer hydrogenation between tetralin and butadiene

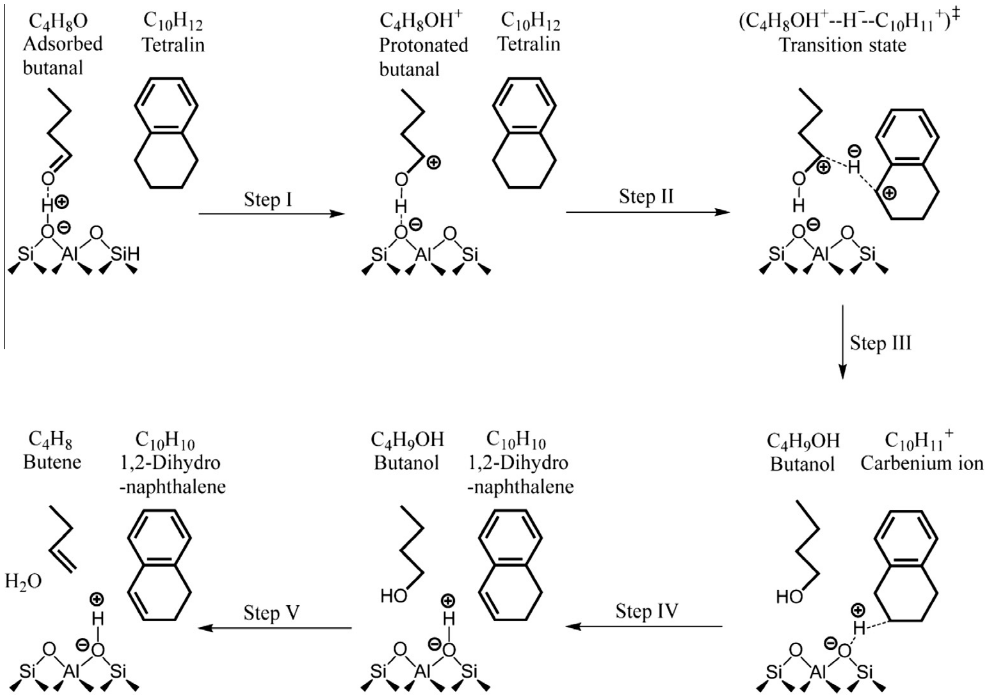

Scheme 2. A proposed mechanism for inter-molecular hydride transfer from tetralin to protonated butanal (the kinetically-relevant step for Pathway 2).

Table 4
Transfer hydrogenation rates of butanal ($r_{TH,C_4H_8O-tetralin}$), butadiene ($r_{TH,C_4H_6-tetralin}$), and butene ($r_{TH,C_4H_8-tetralin}$) by tetralin on H-FAU at 573 K.

Reaction	**Rate** (mmol (mol H^+ s)$^{-1}$)[a]	
$C_4H_8O + C_{10}H_{12} \rightarrow C_4H_8 + C_{10}H_{10} + H_2O$	$r_{TH,C_4H_8O-tetralin}$[b] ($r_{Intra,C_4H_8O-tetralin} - r_{Intra,C_4H_8O}$)	0.27
$C_4H_6 + C_{10}H_{12} \rightarrow C_4H_8 + C_{10}H_{10}$	$r_{TH,C_4H_6-tetralin}$[c] ($r_{Dehy,C_4H_8O} - r_{Dehy,C_4H_8O-tetralin}$)	4.8×10^{-3}
$C_4H_8 + C_{10}H_{12} \rightarrow C_4H_{10} + C_{10}H_{10}$	$r_{TH,C_4H_8-tetralin}$[d]	1.1×10^{-3}

[a] All rates were measured on H-FAU at 573 K, 1.1 kPa butanal, 0.08 kPa tetralin (if added), space velocity = 0.0074 mol butanal (mol H^+ s)$^{-1}$, *time-on-stream* = 125 min.

[b] Rate for tetralin-to-butanal transfer hydrogenation, $r_{TH,C_4H_8O-tetralin}$, is given by the increase in the rate of butene formation upon tetralin incorporation ($r_{Intra,C_4H_8O-tetralin} - r_{Intra,C_4H_8O}$), according to Eq. (8).

[c] Rate for tetralin-to-butadiene transfer hydrogenation, $r_{TH,C_4H_6-tetralin}$, is given by the decrease in the net rate of butadiene formation upon tetralin incorporation, according to the equation: $r_{TH,C_4H_6-tetralin} = r_{Dehy,C_4H_8O} - r_{Dehy,C_4H_8O-tetralin}$.

[d] Rate for tetralin-to-butene transfer hydrogenation, $r_{TH,C_4H_8-tetralin}$, is given by the rate of butane (C_4H_{10}) formation.

thermodynamically favorable (to be discussed in Section 3.3). Nevertheless, the rate of butadiene (C_4H_6) transfer hydrogenation by tetralin ($r_{TH,C_4H_6-tetralin}$) is approximately two orders of magnitude lower than the incremental rate of butene formation ($r_{Intra,C_4H_8O-tetralin} - r_{Intra,C_4H_8O}$) [4.8 µmol C_4H_6 (mol H^+ s)$^{-1}$ vs. 270 µmol C_4H_8 (mol H^+ s)$^{-1}$, 573 K, Table 4]. Such marked differences in rate magnitude are caused by the much lower pressures and proton affinity (*PA*) for butadiene than butanal (1.5 Pa vs. 1.1 kPa and 783.0 kJ mol^{-1} vs. 792.7 kJ mol^{-1} [31], respectively) and by the concomitant lower coverages of protonated butadiene than butanal at the H^+ sites. This result confirms that butadiene hydrogenation would not affect butanal transfer hydrogenation rate. Similarly, the consumption of the butene (C_4H_8) via its transfer hydrogenation that forms butane (C_4H_{10}) is also negligible, as the rate ($r_{TH,C_4H_8-tetralin}$) is less than 0.5% of the incremental rate of butene formation [1.1 µmol C_4H_{10} (mol H^+ s)$^{-1}$ vs. 270 µmol C_4H_8 (mol H^+ s)$^{-1}$, Table 4].

In contrast to the intra-molecular C=C bond formation (Eq. (1)) and isomerization-dehydration (Eq. (2)) reactions, tetralin incorporation did not perturb the inter-molecular C=C bond formation (Pathway 1 in Scheme 1, labeled ◆ in Figs. 3a and 3b) and Tishchenko esterification-ketonization (Pathway 4, labeled ■ in Figs. 3a and 3b) reactions. The extents of promotion for these reactions, as described by $\alpha_{j,tetralin}$ and $\alpha_{j,tetralin\text{-}ad}$ (j = Inter or Tish, the proportionality constants in Eqs. (5a) and (5b)), are nearly zero on H-FAU, with or without adamantane incorporation. $\alpha_{Inter,tetralin}$ and $\alpha_{Inter,tetralin\text{-}ad}$ are -0.4 ± 0.2 kPa^{-1} and -0.5 ± 0.3 kPa^{-1}, whereas the $\alpha_{Tish,tetralin}$ and $\alpha_{Tish,tetralin\text{-}ad}$ are -1.3 ± 0.3 kPa^{-1} and -0.6 ± 0.1 kPa^{-1}, respectively, as listed in Table 2. The near zero extents of promotion for these reactions ($\alpha_{j,tetralin}$ or $\alpha_{j,tetralin\text{-}ad}$, j = Inter or Tish) reflect the insensitivity of $C_8H_{14}O$ and C_7H_{14} formation rates to tetralin and adamantane pressures. Taken together, we conclude that tetralin addition and hydride transfer catalysis alter neither the identity of most abundant surface intermediates nor the kinetically-relevant steps during butanal deoxygenation reactions.

The direct nature of the hydrogen transfer reaction was probed with tetralin, tetralin-butanal, and hydrogen-butanal reactions on H-FAU (at 573 K) and the hydrogen transfer rates in these mixtures are summarized in Table 3. In the tetralin-butanal mixture (0.08 kPa tetralin, 1.1 kPa butanal), the rate of tetralin dehydrogenation, defined as the total rate of naphthalene formation via transfer dehydrogenation and acid catalyzed dehydrogenation (Steps A and B1), is 2.7 times of that with tetralin (0.08 kPa tetralin) as the sole reactant (Step B1), as shown in Table 3. This result suggests that acid catalyzed tetralin dehydrogenation (Step B1), which occurs via the initial binding of a H atom from the tetralin to a H^+ site in a carbocationic transition state followed by H_2 desorption and the formation of a secondary carbenium ion [32–36], has comparable but yet slightly smaller reactivities than tetralin transfer dehydrogenation (Step A). The transfer dehydrogenation involves a direct, inter-molecular H transfer step that shuffles hydride ions (H^-) from tetralin to protonated butanal, without the involvement of H_2 as the intermediate. A separate experiment with H_2 incorporation showed no rate enhancement for butene formation: the C_4H_8O hydrogenation rate with H_2 ($r_{\mathrm{Hydro,C_4H_8O-H_2}}$, Step B2, Table 3) is ~7 μmol (mol H^+ s)$^{-1}$. This rate in butanal-H_2 mixture is <2% higher than that in butanal (without H_2) and corresponds to a $r_{\mathrm{Intra,C_4H_8O-H_2}}(r_{\mathrm{Intra,C_4H_8O}})^{-1}$ value of 1.02 (90 H_2/C_4H_8O feed ratio, 573 K). Thus, diatomic H_2, even if formed, did not participate in catalytic turnovers. Based on these results, we rule out the kinetic significance of the indirect hydrogenation route, which requires an initial stepwise tetralin dehydrogenation that forms H_2 followed by its addition to butanal (Steps B1 and B2, Table 3). Instead, inter-molecular H transfer must occur via direct transfer hydrogenation that shuffles hydride ions from tetralins to protonated butanals.

3.3. Catalytic effects of alkanal molecular size and local acid site confinements on transfer hydrogenation reactions

Transfer hydrogenation proposed in Scheme 2 involves tetralin ($C_{10}H_{12}$) and protonated alkanal ($C_nH_{2n}OH^+$) as a hydride donor-acceptor pair in a carbonium ion transition state [7,9], $(C_nH_{2n}OH^+\text{--}H^-\text{--}C_{10}H_{11}^+)^\ddagger$. We postulate that the stability of the hydride transfer transition state is dictated by the difference in hydride ion affinities between the carbenium ions of the hydride donor ($C_{10}H_{11}^+$) and the hydride acceptor (protonated alkanals, $C_nH_{2n}OH^+$), denoted as $\Delta HIA_{C_{10}H_{11}^+-C_nH_{2n}OH^+}$:

$$\Delta HIA_{C_{10}H_{11}^+-C_nH_{2n}OH^+} = HIA_{C_{10}H_{11}^+} - HIA_{C_nH_{2n}OH^+} \tag{7}$$

$HIA_{C_{10}H_{11}^+}$ and $HIA_{C_nH_{2n}OH^+}$ denote the hydride ion affinities of $C_{10}H_{11}^+$ and $C_nH_{2n}OH^+$, respectively. As an example, the difference in hydride ion affinities between $C_{10}H_{11}^+$ and $C_4H_8OH^+$, $\Delta HIA_{C_{10}H_{11}^+-C_4H_8OH^+}$, is −13.7 kJ mol^{-1} for the case of butanal deoxygenation. Similarly, the difference in hydride ion affinities between $C_{10}H_{11}^+$ and either $C_3H_6OH^+$, $C_5H_{10}OH^+$, or $C_6H_{12}OH^+$ are −22.5, −10.2, or −7.0 kJ mol^{-1} for the cases of propanal, pentanal, and hexanal deoxygenation, respectively (see Sec. S3 and Table S1 in Appendix for $HIA_{C_{10}H_{11}^+}$ and $HIA_{C_nH_{2n}OH^+}$ estimation). A more negative $\Delta HIA_{C_{10}H_{11}^+-C_nH_{2n}OH^+}$ value indicates a thermodynamically more stable product and thus a lower activation barrier to evolve the carbonium ion transition state, as expected from the Brønsted-Evans-Polanyi relation, and a higher hydride transfer rate. The rates of transfer hydrogenation with tetralin or cyclohexadiene (chd) as the H-donor and alkanal ($C_nH_{2n}O$, n = 3–6) as the H-acceptor, $r_{\mathrm{TH},C_nH_{2n}O-D}$ (D = tetralin or chd), are isolated by subtracting the site-time-yields of alkene (C_nH_{2n}) in $C_nH_{2n}O$ feed ($r_{\mathrm{Intra},C_nH_{2n}O}$) from those in $C_nH_{2n}O$-tetralin or $C_nH_{2n}O$-cyclohexadiene feed mixture ($r_{\mathrm{Intra},C_nH_{2n}O-D}$), measured on H-FAU zeolites at 573 K:

$$r_{\mathrm{TH},C_nH_{2n}O-D} = r_{\mathrm{Intra},C_nH_{2n}O-D} - r_{\mathrm{Intra},C_nH_{2n}O} \tag{8}$$

$r_{\mathrm{TH},C_nH_{2n}O-D}$ is proportional to the H-donor pressure P_D (D = tetralin or chd) via a proportionality constant $k_{\mathrm{TH},C_nH_{2n}O-D}$, which is also the rate constant for transfer hydrogenation between the H-donor D and alkanals $C_nH_{2n}O$:

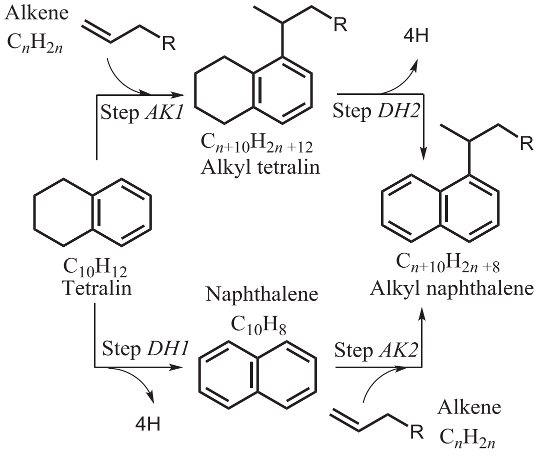

Scheme 3. Reaction network for C_nH_{2n}-tetralin (naphthalene) alkylation.

$$r_{\mathrm{TH},C_nH_{2n}O-D} = k_{\mathrm{TH},C_nH_{2n}O-D}P_D \tag{9}$$

as also indicated from the linear relation in Eqs. (5a)–(5c) and shown in Figs. 3a–3c. $k_{\mathrm{TH},C_nH_{2n}O-D}$ is also the rate constant for the kinetically-relevant nucleophilic attack of the H-donor D (e.g. tetralin) onto the protonated alkanal (e.g. C_4H_8O) via the formation of bimolecular carbocationic transition state, as shown in Step II of Scheme 2.

It was noted that the reactions of alkanal ($C_nH_{2n}O$)-tetralin ($C_{10}H_{12}$) mixtures on H-FAU produced alkyl tetralins ($C_{n+10}H_{2n+12}$) and alkyl naphthalenes ($C_{n+10}H_{2n+8}$), which, however, were not detected in the reaction of alkanal ($C_nH_{2n}O$) alone. It is known that alkene can undergo electrophilic alkylation reaction with aromatics on acidic zeolites [37–41]. Therefore, we speculate that alkene (C_nH_{2n}) formed from alkanal transfer hydrogenation could undergo alkylation reaction with either the tetralin ($C_{10}H_{12}$) or its dehydrogenation product, naphthalene ($C_{10}H_8$), to produce alkyl tetralins ($C_{n+10}H_{2n+12}$) or alkyl naphthalenes ($C_{n+10}H_{2n+8}$), respectively, as shown in Steps *AK1* and *AK2* in Scheme 3. These alkylation reactions consumed the alkene (C_nH_{2n}) and decreased the net rate of

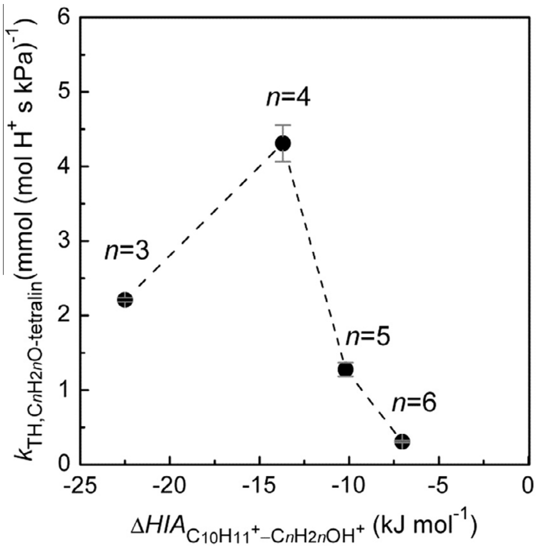

Fig. 4. Rate constants for tetralin-to-alkanal ($C_nH_{2n}O$) transfer hydrogenation ($k_{\mathrm{TH},C_nH_{2n}O-\mathrm{tetralin}}$, Eq. (9), n = 3–6) on H-FAU as a function of the hydride ion affinity difference between the protonated alkanal ($C_nH_{2n}OH^+$) and the carbenium ion of tetralin ($C_{10}H_{11}^+$) (the hydride ion affinity difference is given by Eq. (7)) [573 K, 1,1 kPa alkanal, 0.08–0.16 kPa tetralin, space velocity 0.0074 mol alkanal (mol H^+ s)$^{-1}$].

alkene formation from alkanal transfer hydrogenation. Therefore, the rate for the intra-molecular C=C bond formation in the alkanal-tetralin feed mixture, $r_{\text{Intra},C_nH_{2n}O\text{–tetralin}}$, was determined from the total rates of alkene (C_nH_{2n}), alkyl tetralin ($C_{n+10}H_{2n+12}$), and alkyl naphthalene ($C_{n+10}H_{2n+8}$) formation.

Fig. 4 shows the rate constant $k_{\text{TH},C_nH_{2n}O\text{–tetralin}}$ for different alkanals ($C_nH_{2n}O$, $n = 3–6$) as a function of the hydride ion affinity differences, $\Delta HIA_{C_{10}H_{11}^+–C_nH_{2n}OH^+}$. As the carbon number of alkanal decreases from six to four, their hydride ion affinity ($HIA_{C_nH_{2n}OH^+}$) increases from 941.1 to 947.8 kJ mol^{-1} and thus the $\Delta HIA_{C_{10}H_{11}^+–C_nH_{2n}OH^+}$ concomitantly decreases from −7.0 to −13.7 kJ mol^{-1} (Table S1, in Sec. S3 of Appendix). The more negative hydride ion affinity difference leads to stronger C_nH_{2n}-OH^+--H^- bond and more stable $(C_nH_{2n}OH^+\text{--}H^-\text{--}C_{10}H_{11}^+)^‡$ structure at the transition state and in turn to higher $k_{\text{TH},C_nH_{2n}O\text{–tetralin}}$ values. This trend, however, does not apply for propanal (C_3H_6O). Despite the more negative hydride ion affinity difference for propanal than butanal ($\Delta HIA_{C_{10}H_{11}^+–C_3H_6OH^+} = -22.5$ kJ mol^{-1} vs. $\Delta HIA_{C_{10}H_{11}^+–C_4H_8OH^+} = -13.7$ kJ mol^{-1}), the rate of transfer hydrogenation is lower [$k_{\text{TH},C_3H_6O\text{–tetralin}} = 2.21 \pm 0.03$ mmol (mol H^+ s kPa)$^{-1}$ vs. $k_{\text{TH},C_4H_8O\text{–tetralin}} = 4.3 \pm 0.2$ mmol (mol H^+ s kPa)$^{-1}$, Fig. 4]. This exceptional activity trend for propanal transfer hydrogenation is probably related to the solvation effects of the H^+ site local confinement on the stability of the hydride transfer transition state.

Kinetic investigations of hydride transfer from isobutane to C_3 and C_6 alkoxides during propene oligomerization on solid Brønsted acids show a direct relation between hydride transfer rates and the stabilities and concentrations of hydride ion acceptors [42]. The hydride transfer to C_3 and C_6 alkoxides that forms propane and hexane, respectively, is much less effective for C_3 than C_6 alkoxides, because of the smaller van der Waals stabilizations and thus lower concentrations of C_3 than C_6 alkoxides [42]. These hydride transfer reactivity trends for C_3 and C_6 alkoxides [42] are in the exact opposite to those between alkanal and tetralin (in Fig. 4), because their kinetically-relevant steps differ: the hydride transfer between isobutane and C_3 (or C_6) alkoxides during propene oligomerization is governed by the formation of alkoxides as the H-acceptors [42], but this is not the case between tetralin and C_3—C_6 alkanals. The latter is not limited by the formation of H-acceptor ($C_nH_{2n}OH^+$), because the H^+ sites are already populated by $C_nH_{2n}OH^+$ as the most abundant surface intermediates. Instead, it is limited by the bi-molecular reactions between the hydride donor and acceptor pair to evolve the carbonium ion transition state $(C_nH_{2n}OH^+\text{--}H^-\text{--}C_{10}H_{11}^+)^‡$ (Step II, Scheme 2). The preferential occupation of the H^+ site by alkanals is confirmed from chemical titrations with alkanals [1,6], first order dependence of the parallel, bi-molecular alkanal condensation reaction on the alkanal pressure (Step 1, Scheme 1) [1,6], and the infrared spectroscopic study of butanal adsorption on H-FAU, which shows the disappearance of the O—H stretching bands at 3625 cm^{-1} (in supercages) and 3563 cm^{-1} (in beta cages) and the concomitant appearance of C=O stretching bands at 1675–1685 cm^{-1} [25].

One could not rule out the effects of local structural confinements on these reactivity trends within the alkanal homologues, as such confinements may stabilize the alkanals as well as the transition states: it is plausible that $(C_4H_8OH^+\text{--}H^-\text{--}C_{10}H_{11}^+)^‡$ transition state may be stabilized more than $(C_3H_6OH^+\text{--}H^-\text{--}C_{10}H_{11}^+)^‡$ through larger van der Waals interactions, thus leading to the higher transfer hydrogenation reactivities for C_4H_8O than C_3H_6O (Fig. 4). Similar solvation effects caused by local confinements have been reported for hydride transfer in solid acid catalyzed dimethyl ether homologation [14] and n-pentane cracking [13]. In dimethyl ether homologation, large-pore FAU and BEA zeolites exhibit higher selectivities to triptane than mesoporous SiO_2-Al_2O_3 and medium-pore MFI zeolites, because the pores and cages in FAU and BEA zeolites provide the required physical dimensions as the "right fit" that solvate and stabilize the hydride transfer and methylation transition states to a larger extent than the mesoporous SiO_2-Al_2O_3 and medium-pore MFI zeolites, thus favoring the chain termination to C_7 product (triptane) [14]. In n-pentane cracking, zeolites with cavity volumes of about 0.2 nm^3 [e.g., CIT-1 (0.211 nm^3) and MCM-68 (0.182 nm^3)] were found to be the most active ones in catalyzing the hydride transfer from n-C_5H_{12} to $C_2H_5^+$, $C_3H_7^+$, or $C_4H_9^+$ carbenium ions, which forms alkanes (e.g., C_2H_6, C_3H_8, or C_4H_{10}, respectively), likely because the cavity volumes of these zeolites and the bi-molecular transition states are of comparable dimensions: the volumes for $C_2H_5^+$-n-C_5H_{10}, $C_3H_7^+$-n-C_5H_{10}, and $C_4H_9^+$-n-C_5H_{10} fragments were estimated to be 0.182, 0.203, and 0.224 nm^3, respectively [13]. These effects of site confinement on alkanal transfer hydrogenation are probed with butanal reactions on H^+ sites confined to different extents-in medium pore straight or zig-zag channels of MFI structures (5.4 Å), in supercages (diameter of 11.8 Å) and 12-member ring windows (7.4 Å) of FAU structures, or dispersed on the surfaces of $H_4SiW_{12}O_{40}$ clusters that are then immobilized on mesoporous silica (without molecular scale confinements). Partially confined FAU structures exhibit much higher transfer hydrogenation reactivities than the smaller pore MFI zeolites and unconfined $H_4SiW_{12}O_{40}$ clusters. First, H-FAU promotes tetralin-to-butanal transfer hydrogenation to the largest extent among these catalysts, as indicated by the much larger $\alpha_{\text{Intra,tetralin}}$ values (Eq. (5a), 16.1 ± 0.2 kPa^{-1} on H-FAU vs. 1.3 ± 0.2 kPa^{-1} and 0.7 ± 0.3 kPa^{-1} on H-MFI and $H_4SiW_{12}O_{40}$, respectively, Table 2). Second, the selectivities to intra-molecular C=C bond formation (Pathway 2), S_{Intra,C_4H_8O}, are much higher on H-MFI and H-FAU than on $H_4SiW_{12}O_{40}$ ($S_{\text{Intra},C_4H_8O} = 0.27$ and 0.37 vs. 0.01, Table 1), an indication that butanal transfer hydrogenation is promoted within the confined pores and cages of molecular dimensions than on the unconfined $H_4SiW_{12}O_{40}$ clusters. We hypothesize that the partially confined environment in H-FAU (diameter of supercages = 11.8 Å) could stabilize the $(C_4H_8OH^+\text{--}H^-\text{--}C_{10}H_{11}^+)^‡$ carbonium ion type transition state to a greater extent than H-MFI and $H_4SiW_{12}O_{40}$. The pores of H-MFI (5.4 Å) are too small to accommodate the bi-molecular transition state complex consisting of fragments from a large H-donor (e.g., tetralin, kinetic diameter > 6.2 Å [43]) and the protonated butanal (~4.5 Å). Such a structure permits only smaller compounds acting as the H-donors (e.g., 5,6-dimethyl-1,3-cyclohexadiene), thus leading to lower transfer hydrogenation reactivities and lower selectivities on H-MFI than on H-FAU ($S_{\text{Intra},C_4H_8O} = 0.27$ on H-MFI vs. 0.37 on H-FAU, Table 1).

The fraction of C_7-C_9 aromatics formed upon the dehydrogenation-transalkylation of C_8 cycloalkadienes, is higher on H-MFI (16%, Fig. 2c) than on H-FAU (10%, Fig. 2a). In contrast, the fraction of the dehydrogenated C_{11}—C_{17} aromatic species are much lower on H-MFI (45%, Fig. 2c) than on H-FAU (70%, Fig. 2a). These distinct product distributions suggest the difference in molecular dimension and identity of the hydrogen donors: the primary H-donors in medium pore H-MFI are the smaller hydrocarbon species (e.g. C_8 alkyl cyclohexadienes), whereas in the large pore H-FAU are larger aromatics, ranging from C_8 to C_{17}.

This size requirement for H-donor was probed by incorporating cyclohexadiene or tetralin as the H-donor for butanal transfer hydrogenation. The kinetic diameter of cyclohexadiene is estimated to be ~5.4–5.9 Å [44]; therefore, it can access both the medium pores (5.4 Å) of H-MFI and the large pores (7.4 Å) of H-FAU and act as an effective H-donor on both catalysts ($\alpha_{\text{Intra,chd}} = 14.4 \pm 0.8$ and 29.0 ± 2.0 kPa^{-1} on H-MFI and H-FAU, respectively, Table 2).

In contrast, tetralin (∼6.2 Å [45]) can access only the large pores of H-FAU but not the medium pore of H-MFI; as a result, tetralin promotes only the butanal transfer hydrogenation on H-FAU ($\alpha_{\mathrm{Intra,tetralin}} = 16.1 \pm 0.2$ and $1.3 \pm 0.2\ \mathrm{kPa}^{-1}$ on H-FAU and H-MFI, respectively, Table 2). The rate constant for cyclohexadiene-to-butanal transfer hydrogenation, $k_{\mathrm{TH,C_4H_8O-chd}}$, is lower on H-MFI than on H-FAU [2.8 ± 0.4 vs. 6.8 ± 0.3 mmol (mol H^+ s kPa)$^{-1}$, Table 2]. This might be caused by the steric constraints in H-MFI that destabilize the bulky transition state $(C_4H_8OH^+\text{--}H^-\text{--}C_6H_7^+)^{\ddagger}$ of hydride transfer, as the pores of H-MFI (5.4 Å) have similar dimensions with the kinetic diameter of cyclohexadiene (∼5.4–5.9 Å). The steric constraints may partially compensate the solvation effects, making the transition state less stable in the medium pores of H-MFI than the supercages of H-FAU.

In contrast to the H^+ sites confined within the microporous structure of H-MFI and H-FAU zeolites, the unconfined H^+ sites on $H_4SiW_{12}O_{40}$ clusters produce strictly aromatics with 12 or 16 carbon atoms (Fig. 2d) as a result of cyclization-dehydration of trimeric ($C_{12}H_{20}O$) and tetrameric ($C_{16}H_{26}O$) alkenals produced from the inter-molecular C=C bond formation steps, respectively. These aromatics do not undergo sequential transalkylation on $H_4SiW_{12}O_{40}$ clusters, as transalkylation requires confined reaction environment. The lack of confinement in $H_4SiW_{12}O_{40}$ clusters also inhibits the hydride transfer step; thus, only a small fraction (22%) of the aromatics undergo dehydrogenation, as shown in Fig. 2d. For this reason, tetralin does not promote butanal transfer hydrogenation on $H_4SiW_{12}O_{40}$, resulting in small $\alpha_{\mathrm{Intra,tetralin}}$ value of $0.7 \pm 0.3\ \mathrm{kPa}^{-1}$ (Table 2). Cyclohexadiene as a more effective H-donor promotes butanal transfer hydrogenation on $H_4SiW_{12}O_{40}$, resulting in a positive $\alpha_{\mathrm{Intra,chd}}$ value of $9.3 \pm 0.3\ \mathrm{kPa}^{-1}$ (Table 2), because its carbenium ion has a much lower hydride ion affinity than that of tetralin ($HIA_{C_6H_7^+} = 907.2\ \mathrm{kJ\ mol^{-1}}$ vs. $HIA_{C_{10}H_{11}^+} = 934.1\ \mathrm{kJ\ mol^{-1}}$, Table S1, Appendix); thus, hydride abstraction is energetically more favorable from cyclohexadiene than tetralin. Despite the promotional effects, the rate constant for cyclohexadiene-to-butanal transfer hydrogenation, $k_{\mathrm{TH,C_4H_8O-chd}}$, is much lower on $H_4SiW_{12}O_{40}$ than on H-FAU and H-MFI [0.52 ± 0.03 vs. 6.8 ± 0.3 and 2.8 ± 0.4 mmol (mol H^+ s kPa)$^{-1}$, respectively, Table 2], an indication that the unconfined H^+ sites on $H_4SiW_{12}O_{40}$ are much less effective for transfer hydrogenation.

4. Conclusions

The transfer hydrogenation of alkanal ($C_nH_{2n}O$) occurs on Brønsted acid sites via a kinetically-relevant hydride transfer step that shuffles an hydride ion from a hydride donor to a protonated alkanal, followed by rapid H_2O removal and the concomitant creation of an intra-molecular C=C bond in the alkanal reactant. The reaction forms an alkene (C_nH_{2n}) in catalytic sojourns that retain the carbon backbone of alkanal. The hydride transfer step involves a bi-molecular $(C_nH_{2n}OH^+\text{--}H^-\text{--}R'H^+)^{\ddagger}$ transition state consisted of a hydride donor (hydrocarbon species, $R'H_2$) and acceptor (protonated alkanal, $C_nH_{2n}OH^+$) pair, with both fragments sharing a hydride ion, similar to those previously found for the hydride transfer between alkane and alkoxide (or the related carbenium ion) in confined, microporous structures. The rates of hydride ion transfer vary linearly with the partial pressure of H-donors, identified to be the larger hydrocarbon species (e.g., alkyl tetralins), produced from the parallel inter-molecular C—C bond formation and ring closure steps, and confirmed here by tetralin, cyclohexadiene, and adamantane (a co-catalyst) incorporation which specifically promotes transfer hydrogenation among the various pathways of alkanal deoxygenation.

The rate constants for transfer hydrogenation are correlated to the hydride ion affinity difference between the carbenium ions of the H-donors ($R'H^+$) and the protonated alkanals ($C_nH_{2n}OH^+$), as it dictates the heat of the hydride transfer reaction and in turn the stability of the hydride transfer transition state. Smaller alkanals with higher hydride ion affinities exhibit larger transfer hydrogenation rates ($C_4 > C_5 > C_6$). An exception is propanal-despite its higher hydride ion affinity, it appears to be much less reactive in the transfer hydrogenation than butanal, a phenomenon likely caused by the smaller transition state for propanal than for larger alkanals and its lesser extent of solvation in the FAU cages.

The transfer hydrogenation occurs much faster on H^+ sites confined within the supercages of FAU zeolites than those in the medium pore MFI zeolites or dispersed on unconfined $H_4SiW_{12}O_{40}$ Keggin structures, likely because partially confined environments in the FAU supercages solvate and stabilize the bi-molecular $(C_nH_{2n}OH^+\text{--}H^-\text{--}R'H^+)^{\ddagger}$ transition state via van der Waals interactions. As the alkanal size increases from C_3 to C_6, the transition state may be stabilized by their larger van der Waals interactions with the zeolitic wall, but such stabilizations are offset by the destabilization caused by steric hindrances. We hypothesize that the interaction between the transition state and local site environment, together with the variation in the hydride ion affinity of alkanals, leads to the observed reactivity trend of $C_4 > C_3 > C_5 > C_6$ for tetralin-to-alkanal transfer hydrogenation in H-FAU zeolites. These effects of local site structures and the thermochemical properties of reactant determine the reactivity of hydride transfer within the various concomitant catalytic cycles and thus govern the selectivity ratio toward alkenes, dienes, aromatics, and larger oxygenates during alkanal deoxygenation reactions.

Acknowledgments

This study was supported by Natural Sciences and Engineering Research Council of Canada (NSERC), Valmet, Abellon CleanEnergy, Canada Foundation for Innovation (CFI); Y-H. Chin acknowledges Ontario Early Researcher Award Program (ERA), and F. Lin acknowledges Hatch Graduate Scholarship for Sustainable Energy Research and Ontario Graduate Scholarship for supports.

Appendix A. Supplementary material

Supplementary data associated with this article can be found, in the online version, at http://dx.doi.org/10.1016/j.jcat.2016.06.008.

References

[1] F. Lin, Y.-H. Chin, J. Catal. 311 (2014) 244–256.

[2] T.Q. Hoang, X. Zhu, T. Sooknoi, D.E. Resasco, R.G. Mallinson, J. Catal. 271 (2010) 201–208.

[3] T.Q. Hoang, X. Zhu, L.L. Lobban, D.E. Resasco, R.G. Mallinson, Catal. Commun. 11 (2010) 977–981.

[4] A.G. Gayubo, A.T. Aguayo, A. Atutxa, R. Aguado, M. Olazar, J. Bilbao, Ind. Eng. Chem. Res. 43 (2004) 2619–2626.

[5] W. Shen, G.A. Tompsett, R. Xing, W.C. Conner, G.W. Huber, J. Catal. 286 (2012) 248–259.

[6] F. Lin, Y.-H.C. Chin, Unpublished results.

[7] M. Boronat, P. Viruela, A. Corma, J. Phys. Chem. A 102 (1998) 9863–9868.

[8] M. Boronat, P. Viruela, A. Corma, J. Phys. Chem. B 103 (1999) 7809–7821.

[9] V.B. Kazansky, M.V. Frash, R.A.v. Santen, Catal. Lett. 48 (1997) 61–67.

[10] G.M. Mullen, M.J. Janik, ACS Catal. 1 (2011) 105–115.

[11] S. Gronert, J.R. Keeffe, J. Am. Chem. Soc. 127 (2005) 2324–2333.

[12] A. Platon, W. Thomson, Catal. Lett. 101 (2005) 15–20.

[13] A. Miyaji, Y. Iwase, T. Nishitoba, N.Q. Long, K. Motokura, T. Baba, Phys. Chem. Chem. Phys. 17 (2015) 5014–5032.

[14] D.A. Simonetti, R.T. Carr, E. Iglesia, J. Catal. 285 (2012) 19–30.

[15] S. Borghèse, M. Haouas, J. Sommer, F. Taulelle, J. Catal. 305 (2013) 130–134.

[16] V.B. Kazansky, I.N. Senchenya, J. Catal. 119 (1989) 108–120.

[17] I.N. Senchenya, V.B. Kazansky, Catal. Lett. 8 (1991) 317–325.

[18] E.M. Evleth, E. Kassab, H. Jessri, M. Allavena, L. Montero, L.R. Sierra, J. Phys. Chem. 100 (1996) 11368–11374.

[19] T. Prasomsri, R.E. Galiasso Tailleur, W.E. Alvarez, T. Sooknoi, D.E. Resasco, Appl. Catal. A 389 (2010) 140–146.

[20] D.S. Santilli, J. Catal. 99 (1986) 327–334.

[21] E. Dumitriu, V. Hulea, S. Kaliaguine, M.M. Huang, Appl. Catal. A 135 (1996) 57–81.

[22] W. Hoelderich, F. Merger, W.D. Mross, G. Fouquet, US4560822 A, 1985.

[23] H. Kawakami, S. Yoshida, J. Chem. Soc., Faraday Trans. 2 (82) (1986) 1385–1397.

[24] M. Hunger, in: J. Cejka, A. Corma, S. Zones (Eds.), Zeolites and Catalysis: Synthesis, Reactions and Applications, WILEY-VCH Verlag GmbH & Co. KGaA, 2010, pp. 498–535.

[25] Y. Yang, F. Lin, Y.-H.C. Chin, Unpublished results.

[26] C.A. Coulson, S.L. Altmann, Trans. Faraday Soc. 48 (1952) 293–302.

[27] D.A. Simonetti, J.H. Ahn, E. Iglesia, Chem. Cat. Chem. 3 (2011) 704–718.

[28] J. Valyon, J. Engelhardt, F. Lónyi, D. Kalló, Á. Gömöry, Appl. Catal. A 229 (2002) 135–146.

[29] R. Radhakrishan, D.M. Do, S. Jaenicke, Y. Sasson, G.-K. Chuah, ACS Catal. 1 (2011) 1631–1636.

[30] G.J. Hutchings, I.D. Hudson, D. Bethell, D.G. Timms, J. Catal. 188 (1999) 291–299.

[31] E.P.L. Hunter, S.G. Lias, J. Phys. Chem. Ref. Data 27 (1998) 413–639.

[32] J.A. Lercher, R.A. van Santen, H. Vinek, Catal. Lett. 27 (1994) 91–96.

[33] S.R. Blaszkowski, A.P.J. Jansen, M.A.C. Nascimento, R.A. van Santen, J. Phys. Chem. 98 (1994) 12938–12944.

[34] T. Bučko, L. Benco, O. Dubay, C. Dellago, J. Hafner, J. Chem. Phys. 131 (2009) 214508.

[35] I. Milas, M.A.C. Nascimento, Chem. Phys. Lett. 373 (2003) 379–384.

[36] J.H. Yun, R.F. Lobo, J. Phys. Chem. C 118 (2014) 27292–27300.

[37] G. Bellussi, G. Pazzuconi, C. Perego, G. Girotti, G. Terzoni, J. Catal. 157 (1995) 227–234.

[38] A. Corma, V. Martínez-Soria, E. Schnoeveld, J. Catal. 192 (2000) 163–173.

[39] S. Namuangruk, P. Pantu, J. Limtrakul, J. Catal. 225 (2004) 523–530.

[40] C. Perego, P. Ingallina, Catal. Today 73 (2002) 3–22.

[41] S. Siffert, L. Gaillard, B.L. Su, J. Mol. Catal. A: Chem. 153 (2000) 267–279.

[42] M.L. Sarazen, E. Iglesia, Incorporation of light alkanes into alkene oligomerization cycles on solid brønsted acid catalysts, in: 2015 AIChE Annual Meeting, Salt Lake City, 2015.

[43] J. Jae, G.A. Tompsett, A.J. Foster, K.D. Hammonda, S.M. Auerbach, R.F. Lobo, G. W. Huber, J. Catal. 279 (2011) 257–268.

[44] J.-R. Li, R.J. Kuppler, H.-C. Zhou, Chem. Soc. Rev. 38 (2009) 1477–1504.

[45] J. Jae, G.A. Tompsett, A.J. Foster, K.D. Hammond, S.M. Auerbach, R.F. Lobo, G.W. Huber, J. Catal. 279 (2011) 257–268.